Steam methane reforming over bi-metal loaded hemp derived activated carbon-based catalyst for hydrogen production

By

Rashid Minhas

00000319874

Session 2019-2021

Supervised By

Dr. Asif Hussain Khoja

A Thesis Submitted to U.S. – Pakistan Center for Advanced Studies in Energy in partial fulfillment of the requirements for the degree of

MASTERS of SCIENCE

in

THERMAL ENERGY ENGINEERING

U.S. –Pakistan Center for Advanced Studies in Energy (USPCAS-E)

National University of Sciences and Technology (NUST)

H-12, Islamabad 44000, Pakistan

June 2022

Steam methane reforming over bi-metal loaded hemp derived activated carbon-based catalyst for hydrogen production

By

Rashid Minhas

00000319874

Session 2019-2021

Supervised By

Dr. Asif Hussain Khoja

A Thesis Submitted to U.S. – Pakistan Center for Advanced Studies in Energy in partial fulfillment of the requirements for the degree of

MASTERS of SCIENCE

in

THERMAL ENERGY ENGINEERING

U.S.– Pakistan Center for Advanced Studies in Energy (USPCAS-E)

National University of Sciences and Technology (NUST)

H-12, Islamabad 44000, Pakistan

June 2022

THESIS ACCEPTANCE CERTIFICATE

Certified that final copy of MS/MPhil thesis written by Mr. Rashid Minhas, (Registration No. 00000319874), of U.S.-Pakistan Center for Advanced Studies in Energy (USPCASE), NUST has been vetted by undersigned, found complete in all respects as per NUST Statues/Regulations, is in the allowable limits of plagiarism, errors, and mistakes and is accepted as partial fulfillment for award of MS/MPhil degree. It is further certified that necessary amendments as pointed out by GEC members of the scholar have also been incorporated in the said thesis.

Signature: _____

Name of Supervisor: Dr. Asif Hussain Khoja

Date: _____

Signature (HoD TEE): _____

Date: _____

Signature (Principal/Dean): _____

Date: _____

Certificate

This is to certify that work in this thesis has been carried out by **Mr. Rashid Minhas** and completed under my supervision in Fossil Fuels laboratory, USPCAS-E, National University of Sciences and Technology, H-12, Islamabad, Pakistan.

Supervisor: _____

Dr. Asif Hussain Khoja
USPCAS-E
NUST, Islamabad

GEC member 1: _____

Dr. Mustafa Anwar
USPCAS-E
NUST, Islamabad

GEC member 2: _____

Dr. Sehar Shakir
USPCAS-E
NUST, Islamabad

GEC member 3: _____

Dr. Mariam Mehmood
USPCAS-E
NUST, Islamabad

HoD-TEE: _____

Dr. Majid Ali
USPCAS-E
NUST, Islamabad

Principal: _____

Prof. Dr. Adeel Waqas
USPCAS-E
NUST, Islamabad

Acknowledgments

In God I trust. I am thanking Almighty God, for letting me through all the ups and downs. You are the one who let me accomplish my degree. I will always keep trusting on you.

Secondly, I would like to extend my warmest gratitude to my supervisor Dr. Asif Hussain Khoja, without his unstinting support, this work could definitely not be possible. His competent supervision carried me through all the stages towards the completion of this project. I am also grateful to my GEC members for becoming a part of my research and letting my defense be an enjoyable moment, and particularly for your brilliant comments and suggestions on the thesis book and technical manuscript. Thanks to you.

I also owe special thanks to our lab engineers, Mr. Ali Abdullah and Mr. Raja Asim, who were always there to give their utmost support on every ground throughout the entire venture of the research. How can I forget about my lab fellows and colleagues, I will be always indebted to you guys for being a helping hand and particularly for your affable love and support. Last but not least, I am expressing my deepest gratitude to my family and especially my parents for their love and encouragement. Dear Mom and Dad, your prayers and blessings are what sustained me this far.

Dedication

I am dedicating this work to my loving parents, Mr. Muhammad Hussain and Mrs. Muhammad Hussain.

List of Publications

''Steam methane reforming over bimetal loaded hemp derived activated carbon-based catalyst for hydrogen production''. Rashid Minhas [1], Asif Hussain Khoja [1], Salman Raza Naqvi[2], Rahat Javaid[3], Umair Yaqub Qazi[4*], Israf Ud Din[5]

MDPI_Energies(Under Review)(IF=3.25)

ABSTRACT

Where the energy domain is shifting towards more clean and sustainable energy in the wake of environmental deterioration, hydrogen has drawn the main attention as a clean fuel in energy insights. Whereas various natural gas reforming techniques are underway for optimum hydrogen production, the methane steam reforming technique also plays a pivotal role alongside. Catalyst plays a central role in defining the reforming processes. Coke deposition and catalyst deactivation is a technical term that research primarily focuses on to improve catalytic performance. In this study, the hemp leaves-derived activated carbon (AC) loaded Ni-Co catalyst is synthesized by the wet-impregnation method for steam methane reforming (SMR) for optimum hydrogen production. The monometallic and bimetallic metal catalysts are synthesized over activated carbon support with 5wt.% by the wet impregnation method. The fresh and spent catalyst undergoes a series of characterization methods such as X-ray diffractometer (XRD), Scanning electron microscopy (SEM) with Energy dispersive X-ray (EDX), Fourier transform infrared spectroscopy (FTIR), Brunauer-Emmett-Teller analysis (BET) and Thermogravimetric analysis (TGA) for physiochemical studies and catalyst suitability for SMR. The catalytic assessment test of all synthesized material for SMR was carried out in a fixed bed reactor at 750 °C WHSV 2000 mL CH_4 g^{-1} h^{-1} and S/C of 2.0. The catalytic results showed that among all investigated samples monometallic cobalt catalyst (5%Co@AC) recorded best in terms of CH_4 conversion (97.17%) and H_2 production (66.08%) as XRD and SEM results suggest the catalysts with smaller metal crystallites promote a better dispersion of highly porous AC. The Ni/AC, Ni-Co/AC gives the CH_4 conversion (90.28%) and (92.52%) respectively, whereas the H_2 production of Ni/AC and Ni-Co/AC becomes 61.02% and 65.89% respectively.

Keywords: *Steam methane reforming; Hemp; activated carbon; Hydrogen*

Table of Content

List of Figures

List of Tables

List of Abbreviations

AC	Activated Carbon
ATR	Auto Thermal Reforming
BC	Biochar
BET	Brunauer-Emmett-Teller Analysis
CHNS	Carbon, Hydrogen, Nitrogen and Sulphur Analyzer
DFT	Density Functional Theory
DRM	Dry Reforming of Methane
EDX	Energy-Dispersive X-Ray Spectroscopy
FTIR	Fourier Transform Infrared Spectroscopy
GC	Gas Chromatography
GHG	A Greenhouse Gas
IR	Infrared
MT	Million Tons
NPS	Metallic Nanoparticles
POM	Partial Oxidation of Methane
SEM	Scanning Electron Microscopy
SMR	Steam Methane Reforming
SS	Stainless Steel

TCD	Thermal Conductivity Detector
TGA	Thermogravimetric Analysis
TOF	Turnover Frequency
TOS	Time on stream
WGS	Water-Gas-Shift
XRD	X-Ray Diffraction

Chapter 1

Introduction

1.1 Background

Meeting the energy demand for sustainable human development and protecting the environment at the same time from these energy production facilities is a serious challenge for the developing world [1-3]. Therefore, environmental deterioration is the major challenge as demand in the energy sector increases [4-6]. Statistically, nearly 20-40% of the world population lives in regions, where already 1.5 ℃ temperature rise was observed comparatively before the industrial revolution period. Consequently, an onset requirement to decrease greenhouse gas (GHG) emissions that are produced in sectors like power plants, transportation, and agricultural to meet the target of the Paris agreement [7]. The environmental stakeholders are serious about conventional energy production via fossil fuel sources. The greenhouse gas emissions from these conversions contribute to environmental challenges such as global warming and ozone depletion. On the account of these challenges, currently, researchers and scientists focus on the clean production of energy sources in the account of environmental protection call [8-11].

The increasing energy demand and energy security parameter is the major concern of the developing world. The worldwide energy security is very important and it has to provide viable services to its end users. This end-use term determines the quantity of energy production and consequent green gas emission. Enhancing the size of production is not the core issue but also the actual challenge is how to mitigate the climate changes that occur during energy production processes [12]. Clean- environmental-friendly and sustainable energy production is the main attention because of environmental protection calls. In the current scenario, the energy production sector is shifting from conventional fuels into renewable energy sources. However, at the same time, irrespective of conventional fossil fuels energy, some renewable energy sources such as wind energy, and solar radiance energy are not much stable and persistent. The variance of solar radiation because of weather

changes and wind currents also changes on a daily and sessional basis, consequently hampers sustainable energy production [13].

Hydrogen can be created from both renewable and non-renewable sources. The Hydrogen Council is chipping away at the long-term potential of hydrogen deployment in the energy sector. In 2021, the hydrogen demand was calculated as 90 million tons (Mt) [14]. The studies of the hydrogen council guaranteed that hydrogen will cover 18% of worldwide energy interest by 2050 [15]. Hydrogen has great potential to alternate conventional fossil fuels. It is emerging as a clean energy source in various sectors (electricity, heat, or co-generation) [16] because of its environmentally- friendly nature and one of the richest in energy calorific value. Some other interests in hydrogen are; that it is clean energy, abundant in the universe, easy to store, can be easily produced from water, and direct conversion into thermal, mechanical, and electrical energy is possible [17, 18]. Nowadays fuel cell technology is termed the most innovative in the energy sector. In a fuel cell, hydrogen primarily reacts with oxygen, producing only water and plenty of energy. More importantly, unlike fossil fuels, there are not any environmental polluting gases being produced in the process. That is the reason that hydrogen is a promising fuel for energy foresight [19-23].

Studies are underway for clean hydrogen production. Approximately 60% of hydrogen is produced from methane in the current scenario [24]. Some of the prominent processes of hydrogen production are steam methane reforming (SMR) and dry reforming of methane (DRM), partial oxidation reforming (POM), and auto-thermal reforming (ATR) [9]. SMR is widely used in hydrogen production. In 2020, around 50% of hydrogen is produced from SMR alone [25]. Younas et al [24] report that more than 80% of hydrogen is coming from SMR. Methane is a highly stable gas and requires very high energy for its proper use.

1.2 Problem statement

The role of the catalyst is very important in SMR because coke formation during the process is the major issue that consequently deactivates the catalyst performance.

Some noble metals such as Pt, Ru, and Rh turned out to be efficient catalysts because these metals show high reactivity and less carbon deposition. So, their rare availability and high cost are not feasible usages [26-30]. Nickel-based catalysts are widely used on an industrial scale. But, it takes a higher steam: methane molar ratio from 3 to 3.5 for proper gasification and to avoid coke formation [31]. On the other hand, cobalt is a good selection because it is not expensive as noble metal and is readily available. More interestingly, it has a good performance of reactivity and produces a rich synthetic gas ($H_2$and CO) of near ratio to unity [32].

1.3 Research Hypothesis

To synthesize a proper catalyst, a metal is spread over the support to avoid catalyst sintering and to reduce carbon formation [31]. Usually, the carbon starts to deposit at a temperature of 600°C and 800°C throughout the reactions [33].

$$CH_4 \leftrightarrow C + 2H_2 \quad (\Delta H_{298K} = 75kJ/mol) \tag{1}$$

$$2CO \leftrightarrow CO_2 + C \quad (\Delta H_{298K} = 86.2kJ/mol) \tag{2}$$

The equations and represent the chemical reactions of carbon deposition.

As the world is shifting toward a clean energy route, the steam reforming of methane is one of the prominent ways to convert conventional fossil fuels into clean energy sources like hydrogen. The catalyst design is an important parameter that catalyses the process of convert natural gas into hydrogen. The coke formation during the process is the major issue that deactivates the catalyst. Hence, the preparation of proper catalyst is core objective in reforming techniques for hydrogen production.

1.4 Objective of the study

Hemp (cannabis) has great potential for renewable energy alongside several advantages. Firstly, it grows mostly in all environments and climates, and more importantly, it is environment friendly. It has a high biomass content, low cost, mild nutrients to grow, does not require pesticides, effectively large production, and high

dry matter yield [34-36]. hemp grows wildly in different vicinities of Pakistan [34] and the bushes of hemp are mostly seen sprouting the sideways on roads in the capital territory, Islamabad [37]. There is a variety of applications of hemp however on an industrial scale, it has the great advantage of its excellent porous structure. Hemp is essentially used to derive activated carbon which is porous carbon used as adsorbent and hydrogen storage material in energy-related applications and predominantly used as catalyst support and catalyst itself [38, 39].

- Hemp leaves derived activated carbon used as catalyst support for Ni-Co loaded catalyst that is investigated for steam methane reforming
- The physicochemical properties of synthesized material are investigated via various characterization techniques to study physicochemical properties
- 5%Co@AC shows stable CH_4 conversion and H_2 production.
- The physicochemical properties show activated carbon as suitable catalyst support

1.5 Scope of study

The synthesis and analysis of catalysts is the main factor of process engineering. After the preparation of activated carbon from hemp through the chemical activation process, Ni and Co are impregnated for catalyst synthesis, the chemical process is known to be the wet impregnation method. The catalysts are gone through multiple characterization techniques for physiosorbed properties. The catalysts are tested for catalytic activity in a fixed bed reactor for high methane conversion and better hydrogen production. The spent catalysts are also characterized to study material changing parameters. The steps of research are presented in Fig 1.1.

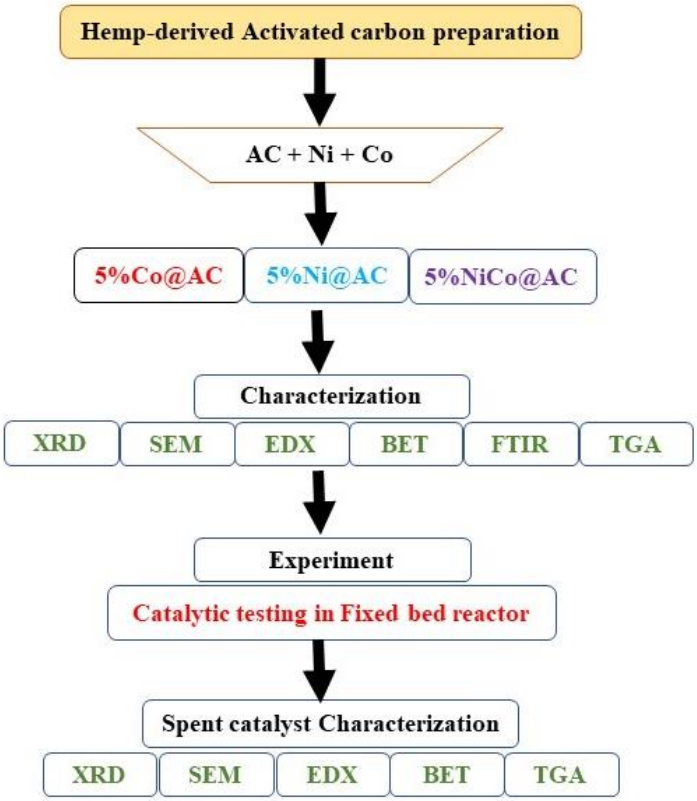

Fig 1.1 The research scope steps

References

1. Morkovkin, D.E., et al. *Formation of a national environmental strategy for the fuel and energy complex*. in *IOP Conference Series: Materials Science and Engineering*. 2019. IOP Publishing.
2. Zhang, J., J. Zheng, and W. Yang, *Green supercapacitor assisted photocatalytic fuel cell system for sustainable hydrogen production.* Chemical Engineering Journal, 2021. **403**: p. 126368.
3. Oznobikhina, L. and E. Pirunova. *Enterprises of the fuel and energy complex-the sphere of high risks and objects of increased industrial danger*. in *IOP Conference Series: Earth and Environmental Science*. 2021. IOP Publishing.
4. Kamran, M., M.R. Fazal, and M. Mudassar, *Towards empowerment of the renewable energy sector in Pakistan for sustainable energy evolution: SWOT analysis.* Renewable Energy, 2020. **146**: p. 543-558.
5. Waris, I. and I. Hameed, *Promoting environmentally sustainable consumption behavior: an empirical evaluation of purchase intention of energy-efficient appliances.* Energy Efficiency, 2020. **13**(8): p. 1653-1664.
6. Papadis, E. and G. Tsatsaronis, *Challenges in the decarbonization of the energy sector.* Energy, 2020: p. 118025.
7. Meisel, K., et al., *Future renewable fuel mixes in transport in Germany under red ii and climate protection targets.* Energies, 2020. **13**(7): p. 1712.
8. Gao, N., et al., *Syngas production via combined dry and steam reforming of methane over Ni-Ce/ZSM-5 catalyst.* Fuel, 2020. **273**: p. 117702.
9. Boyano, A., et al., *Conventional and advanced exergoenvironmental analysis of a steam methane reforming reactor for hydrogen production.* Journal of Cleaner Production, 2012. **20**(1): p. 152-160.
10. Hanif, I., et al., *Fossil fuels, foreign direct investment, and economic growth have triggered CO2 emissions in emerging Asian economies: some empirical evidence.* Energy, 2019. **171**: p. 493-501.

11. Acar, C., I. Dincer, and G.F. Naterer, *Clean hydrogen and power from impure water.* Journal of Power Sources, 2016. **331**: p. 189-197.

12. Grubler, A., et al., *A low energy demand scenario for meeting the 1.5 C target and sustainable development goals without negative emission technologies.* Nature energy, 2018. **3**(6): p. 515-527.

13. Guo, S., et al., *A review on the utilization of hybrid renewable energy.* Renewable and Sustainable Energy Reviews, 2018. **91**: p. 1121-1147.

14. International Energy Agency: IEA, P., *Global Hydrogen Review 2021*. 2021.

15. Safari, F. and I. Dincer, *A review and comparative evaluation of thermochemical water splitting cycles for hydrogen production.* Energy Conversion and Management, 2020. **205**: p. 112182.

16. Capurso, T., et al., *Perspective of the role of hydrogen in the 21st century energy transition.* Energy Conversion and Management, 2022. **251**: p. 114898.

17. Jain, I., *Hydrogen the fuel for 21st century.* International journal of hydrogen energy, 2009. **34**(17): p. 7368-7378.

18. Acar, C. and I. Dincer, *The potential role of hydrogen as a sustainable transportation fuel to combat global warming.* International Journal of Hydrogen Energy, 2020. **45**(5): p. 3396-3406.

19. Bartels, J.R., M.B. Pate, and N.K. Olson, *An economic survey of hydrogen production from conventional and alternative energy sources.* International journal of hydrogen energy, 2010. **35**(16): p. 8371-8384.

20. Zerta, M., et al., *Alternative World Energy Outlook (AWEO) and the role of hydrogen in a changing energy landscape.* International journal of hydrogen energy, 2008. **33**(12): p. 3021-3025.

21. Maggio, G., A. Nicita, and G. Squadrito, *How the hydrogen production from RES could change energy and fuel markets: A review of recent literature.* International Journal of Hydrogen Energy, 2019. **44**(23): p. 11371-11384.

22. Abbas, H.F. and W.W. Daud, *Hydrogen production by methane decomposition: a review.* International journal of hydrogen energy, 2010. **35**(3): p. 1160-1190.

23. Stankiewicz, A., *Energy matters: alternative sources and forms of energy for intensification of chemical and biochemical processes.* Chemical Engineering Research and Design, 2006. **84**(7): p. 511-521.

24. Yang, X., S. Wang, and Y. He, *Review of catalytic reforming for hydrogen production in a membrane-assisted fluidized bed reactor.* Renewable and Sustainable Energy Reviews, 2022. **154**: p. 111832.

25. Pajak, M., et al., *A multiobjective optimization of a catalyst distribution in a methane/steam reforming reactor using a genetic algorithm.* International Journal of Hydrogen Energy, 2020.

26. Zhang, Y., et al., *Steam reforming of methane over Ni/SiO2 catalyst with enhanced coke resistance at low steam to methane ratio.* Catalysis Today, 2015. **256**: p. 130-136.

27. Park, K.S., M.H. Jeong, and J.W. Bae, *Synergy Effects of Cobalt Oxides on Ni/Co-Embedded Al2O3 for Hydrogen-Rich Syngas Production by Steam Reforming of Propane.* Catalysts, 2020. **10**(4): p. 461.

28. Sohrabi, S. and A. Irankhah, *Synthesis, characterization, and catalytic activity of Ni/CeMnO2 catalysts promoted by copper, cobalt, potassium and iron for ethanol steam reforming.* International Journal of Hydrogen Energy, 2021. **46**(24): p. 12846-12856.

29. Etminan, A. and S. Sadrnezhaad, *A two step Microwave-assisted coke resistant mesoporous Ni-Co catalyst for methane steam reforming.* Fuel, 2022. **317**: p. 122411.

30. Ren, J., et al., *Recent progress and perspectives of catalyst design and downstream integration in biomass tar reforming.* Chemical Engineering Journal, 2022. **429**: p. 132316.

31. Lucredio, A.F. and E.M. Assaf, *Cobalt catalysts prepared from hydrotalcite precursors and tested in methane steam reforming.* Journal of power sources, 2006. **159**(1): p. 667-672.

32. Izhab, I., M. Asmadi, and N.A.S. Amin, *Methane dry reforming using oil palm shell activated carbon supported cobalt catalyst: Multi-response optimization.* International Journal of Hydrogen Energy, 2020.

33. Nazari, M. and S.M. Alavi, *An investigation of the simultaneous presence of Cu and Zn in different Ni/Al2O3 catalyst loads using Taguchi design of experiment in steam reforming of methane.* International Journal of Hydrogen Energy, 2020. **45**(1): p. 691-702.

34. Rehman, M.S.U., et al., *Potential of bioenergy production from industrial hemp (Cannabis sativa): Pakistan perspective.* Renewable and sustainable energy reviews, 2013. **18**: p. 154-164.

35. Mo, L., et al., *Hemp Derived Activated Carbon Supported Nanoscale zero–valent Iron as a Heterogeneous Fenton Catalyst for the Treatment of Pulping Effluent.* BioResources, 2020. **15**(3): p. 4996-5011.

36. Sun, W., et al., *Hemp-derived activated carbons for supercapacitors.* Carbon, 2016. **103**: p. 181-192.

37. *How Pakistan is trying to boost industrial hemp production*, in *Deutsche Welle (DW)*. 2020.

38. Guan, Z., et al., *Characterization and preparation of nano-porous carbon derived from hemp stems as anode for lithium-ion batteries.* Nanoscale Research Letters, 2019. **14**(1): p. 1-9.

39. Lupul, I., et al., *Tailoring of porous texture of hemp stem-based activated carbon produced by phosphoric acid activation in steam atmosphere.* Journal of Porous Materials, 2015. **22**(1): p. 283-289.

Chapter 2

Literature Review

2.1 Energy

The increasing energy demand and energy security parameter is the major concern of the developing world. The worldwide energy security is very important and it has to provide viable services to its end users. This end-use term determines the amount of energy production and consequent green gas emission. Enhancing the size of production is not the core issue but also the actual challenge is how to mitigate the climate changes that occur during energy production processes [1]. Clean- environmental-friendly and sustainable energy production is the main attention because of environmental protection calls. In the current scenario, the energy production sector is shifting from conventional fossil fuels to renewable energy sources. However, at the same time, irrespective of conventional fossil fuels energy, some renewable energy sources such as wind energy, and solar radiance energy are not much stable and persistent. The variance of solar radiation because of weather changes and wind currents also changes on a daily and sessional basis, consequently hampers sustainable energy production [2].

Energy is vital and integral part of our lives to perform daily activities. In developing countries, for a long time, fossil fuels have been used as a source of energy (heat and electricity). To date, 80% of energy demand is met by fossil fuels worldwide. As the population of the world increase and the living standards of people changes, consequently, the energy demand also increases. The estimated world population is likely to be reached 10 billion by 2050. Since 1950 the energy demand increased correspondingly to the living standards of the population. In retrospect, this pattern of energy demand has to be at its peak in 2035. Energy security is the major factor, where the governing system in many countries has to ensure the timescale production to its masses. We have enough coal and natural gas reserves for the upcoming two generations, however, petroleum products are estimated to be depleted quicker than coal and natural gas reserves in the world [3-5].

Meeting the energy demand for sustainable human development and to keep intact the environment at the same time from these energy production facilities is a serious challenge for the developing world [6-8]. Therefore, environmental deterioration is the major challenge as demand in the energy sector increases [9-11]. Statistically, nearly 20-40% of the world population lives in regions, where already 1.5 ^{o}C temperature rises was observed comparatively before the industrial revolution period. Consequently, an onset requirement to decrease greenhouse gas (GHG) emissions that are produced in sectors like power plants, transportation, and agricultural to meet the target of the Paris agreement [12]. The environmental stakeholders are serious about conventional energy production via fossil fuel sources. The greenhouse gas emissions from these conversions contribute to environmental challenges such as global warming and ozone depletion. On the account of these challenges, currently, researchers and scientists focus on the clean production of energy sources in the account of environmental protection call [13-16].

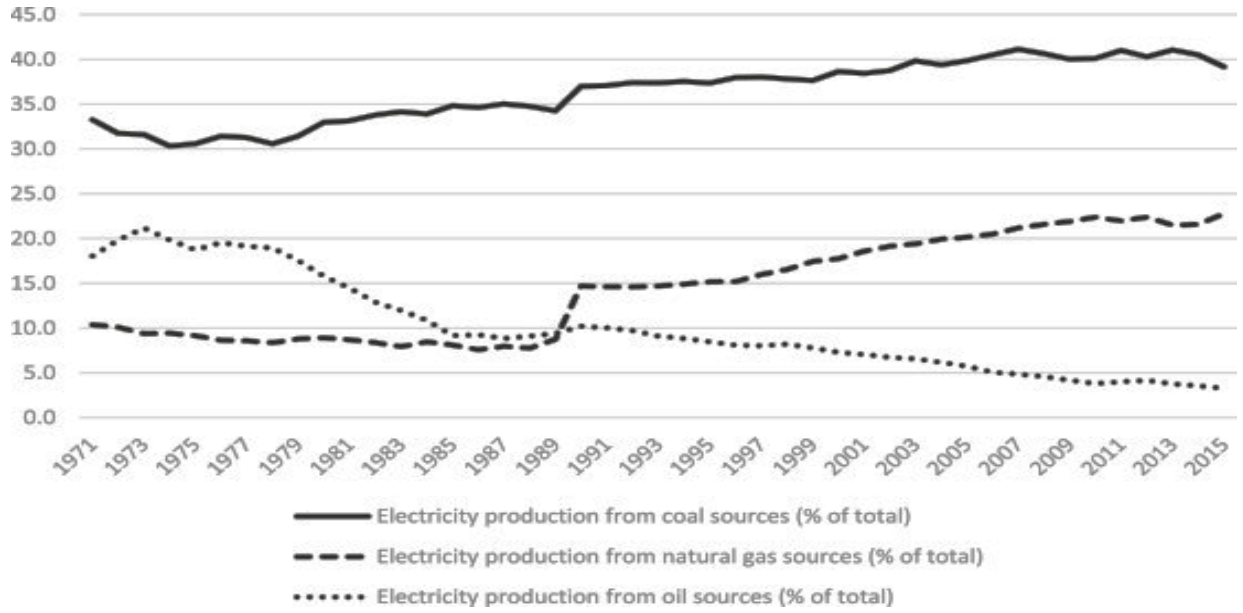

Fig 2.1 The energy production via fossil fuels. Data source: Azmat Ghani[17]

Fig 2.1 represents the yearly energy production in many countries by using fossil fuel energy sources. As clear from the figure, the energy from oil products has decreased gradually, whereas the energy production from coal is significantly increasing. Since the 1970s, the utilization of

coal was estimated to be 30% which has increased to 41% up till the mid-2020s. The coal-burning notoriously produces the main culprit of GHG such as carbon dioxide and carbon monoxide making the severe environmental concerns in the 1980s [17].

2.2 Hydrogen as emerging fuel

Hydrogen has great potential to alternate conventional fossil fuels. It is emerging as a green energy source in various sectors (electricity, heat, or co-generation) [18] since it is environmentally- friendly and at the same time one of the richest in energy calorific value. Some other interests in hydrogen are; that it is green energy, abundantly found in the universe, easy to store, can be easily produced from water such as water splitting, direct conversion into thermal, mechanical, and electrical energy is possible [19, 20]. Nowadays fuel cell technology is termed the most innovative in the energy sector. In a fuel cell, hydrogen primarily reacts with oxygen, producing only water and plenty of energy. More importantly, unlike fossil fuels, there are not any environmental polluting gases being produced in the process. That is the reason that hydrogen is a promising fuel for energy foresight [21-25]. Table 2.1 shows the heat of combustion of some fuels

Table 2.1 The heat of combustion of some fuels

Fuel	**Energy (Kcal/g)**
Hydrogen	34.0
Paraffin	10.3 – 9.8
Petroleum	10.3 – 8.4
Graphite (coal)	7.8
Castor oil	9.4
Wood	4.2

Fig 2.2 shows the current scenario of worldwide hydrogen production from different sources. As clearly, it is very unfortunate that even less than 1% hydrogen comes from renewable ways. Whereas the majority of hydrogen still comes from conventional ways. The Hydrogen Council is working on the long-term potential of hydrogen deployment in the energy sector. In 2019, the hydrogen demand was calculated as 17 million tons (Mt). The studies of the hydrogen council assured that hydrogen will cover 18% of global energy demand by 2050 [26].

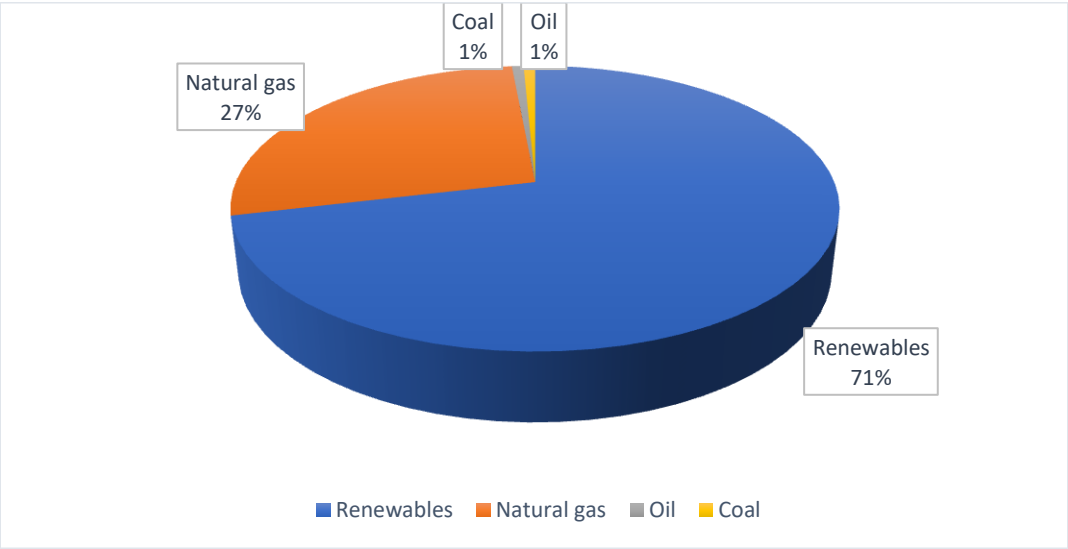

Fig 2.2 Global hydrogen production at current scenario (data taken from[26])

2.3 Hydrogen Production

Hydrogen is the most abundantly found element in the universe and overwhelmingly the 10th most abundant in the earth's crust. It holds the top position in elements of the periodic table and unfortunately does not find in pure form thus preferably produce from hydrogen containing compounds. Although there are enormous ways of hydrogen production. The energy required in its production comes from many means, such as solar energy, wind energy, nuclear energy, geothermal energy, and biomass-derived energies. Fig 2.3 depicts the variety of feedstocks and routes of hydrogen production utilizing various energy sources. Although, the cost of hydrogen production is not very suitable in the current phase. This is one of the reasons to find a route to produce hydrogen at minimum cost and reduce GHG emissions at the same time [5, 27].

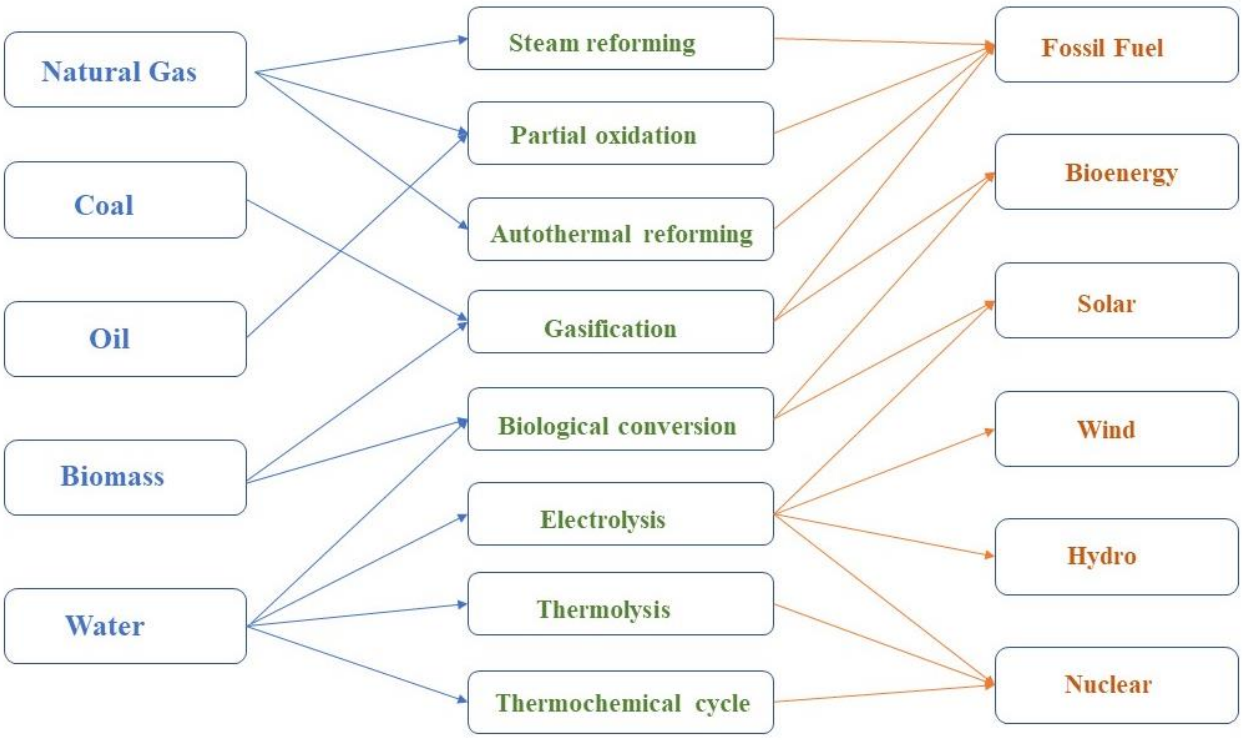

Fig 2.3 The feedstock, routes of generation and source of energy.

Undoubtedly, hydrogen production from renewable resources would be the top priority because of environmental concerns. However, the cost and efficiency of the technologies hamper the great focus on this method. On the account of these matters, to date hydrogen is produced through fossil fuels at a large production scale to meet the global demand [27]. Studies are underway for clean hydrogen production. Approximately 60% of hydrogen is produced from methane in the current scenario [28]. Some of the prominent processes to produce hydrogen are; steam methane reforming (SMR) and dry reforming of methane (DRM), partial oxidation reforming (POM), and auto-thermal reforming (ATR) [14]. SMR is widely used reforming process for hydrogen production. In 2020, around 50% of hydrogen is produced from SMR alone [29]. Younas et al [28] report that more than 80% of hydrogen is coming from SMR.

2.4 Reforming techniques for hydrogen production

Naturally, hydrogen does not exist in pure form and is found in compound forms such as natural gas and other oils. It can be extracted by a series of methods such as.

- bio-oil
- water
- natural gas
- naphtha
- coal gasification
- acetic acid
- alcohol
- glycerol[30]

There are various technologies are being employed for hydrogen production from both renewable and non-renewable (fossil fuels) sources. The reforming techniques of methane are commonly used to produce hydrogen among non-renewable sources.

Non-renewable technologies:

- Steam methane reforming
- Dry methane reforming
- Partial oxidation of methane
- Autothermal methane reforming
- Thermal cracking of methane

Renewable technologies:

The gasification and pyrolysis of biomass feedstock's and water splitting using different renewable energy sources such as wind energy and solar energy are the most prominent technologies for hydrogen production [31]. Approximately 4% of hydrogen is produced by the water electrolysis method. It has its limitation because of the cost of renewable energy sources

[32].

There are further categories of hydrogen based on the production routes.

- **Grey Hydrogen:**

The hydrogen production from fossil fuel sources is termed ‘grey hydrogen’. Therefore, the hydrogen comes from all the reforming techniques where natural gas is used as feedstock is grey hydrogen. SRM is one of them.

- **Blue Hydrogen:**

Blue hydrogen is termed for the hydrogen where CO_2 capturing or carbon dioxide capturing, and storage (CCS) system is deployed for fossil fuel source hydrogen production techniques.

- **Green Hydrogen:**

Similarly, hydrogen comes from renewable energy sources such as biomass gasification and wind-powered, solar-powered, hydral powered water electrolysis is known as green hydrogen[33-35].

- **Brown Hydrogen:**

The hydrogen produces from the coal gasification process is brown hydrogen [35].

2.5 Steam Reforming of Methane

Studies are underway for better hydrogen production. Among all these strategies of reforming, steam methane reforming (SRM) is the most prominent strategy for hydrogen production. The steam reforming of methane (SRM) is widely used in hydrogen production. In 2020, approximately 50% of hydrogen is produced from SRM alone [36, 37]. Whereas, Forbes Magazine estimated roughly 95% of hydrogen production comes from the SMR process alone [38].

In 1924, Neumann and Jacob's first time presented the catalytic reaction of SRM between

methane and water steam for the manufacturing of hydrogen and syngas. Since then, it gained a huge interest in industrial-scale hydrogen production. Ever since the research on good performance material in terms of coke resistant catalyst and tube reactor has never been stopped. Fig 2.4. represents the scheme of methane-conversion strategy for hydrogen production [39].

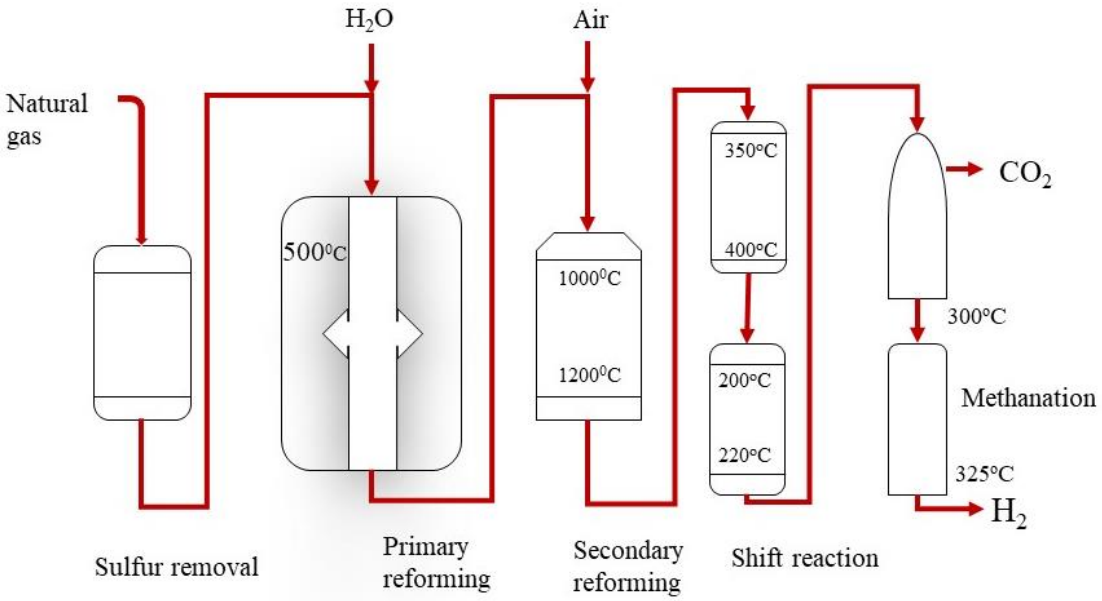

Fig 2.4 Process flow diagram of SMR

According to a model chemical reaction of SRM, the methane reacts with water at an evaluated temperature of roughly 1023-1223K at the pressure of 14-20atm. The reaction is actively endothermic and obtains a good ratio of H_2/CO (approximately 3, which is better for ammonia synthesis and petroleum refining). Methane is a highly stable gas and requires very high energy for its proper use.

The chemical reaction of SRM presented as reaction (3) and (4):

$$CH_4 + H_2O \rightarrow CO + 3H_2 \qquad (\Delta H_{298^\circ C} = 205.9 kJ/mol) \tag{3}$$

$$CH_4 + 2H_2O \rightarrow 2CO_2 + 4H_2 \quad (\Delta H_{298^0C} = 164.7 kJ/mol) \tag{4}$$

The reaction typically occurred at a temperature of 800 °C, in the meantime, a water-gas-shift reaction occurs producing CO_2, which enhances the hydrogen production as represented in reaction (5) [39-43].

$$CO + H_2O \rightarrow CO_2 + H_2 \quad (\Delta H_{298^0C} = -41.1 kJ/mol) \tag{5}$$

Boudouard reaction reaction (6) and methane decomposition equation reaction (7) comprehends the carbon deposition which occurs with time because of the highly endothermic nature of the SRM process [40].

$$2CO \rightarrow C + CO_2 \tag{6}$$

$$CH_4 \rightarrow C + 2H_2 \tag{7}$$

The SRM reactions (1) and (2), are strongly endothermic and operated at more than 800 ºC. Although, the stoichiometric ratio of steam/methane is taken as unity. However, practically the steam ratio is maintained at more than 2.5 to avoid carbon deposition and long-term stability of catalyst [44]. Schematically the conversion of methane into hydrogen occurs at a conventional reformer reactor at an evaluated temperature which is followed by WGS stages at respective high temperatures and low temperatures in a WGS reactor. In the final stage, hydrogen is separated in pressure swing adsorption (PSA) and preferential oxidation reactor (PSA) reactors. The schematic is illustrated below in Fig. 2.5.

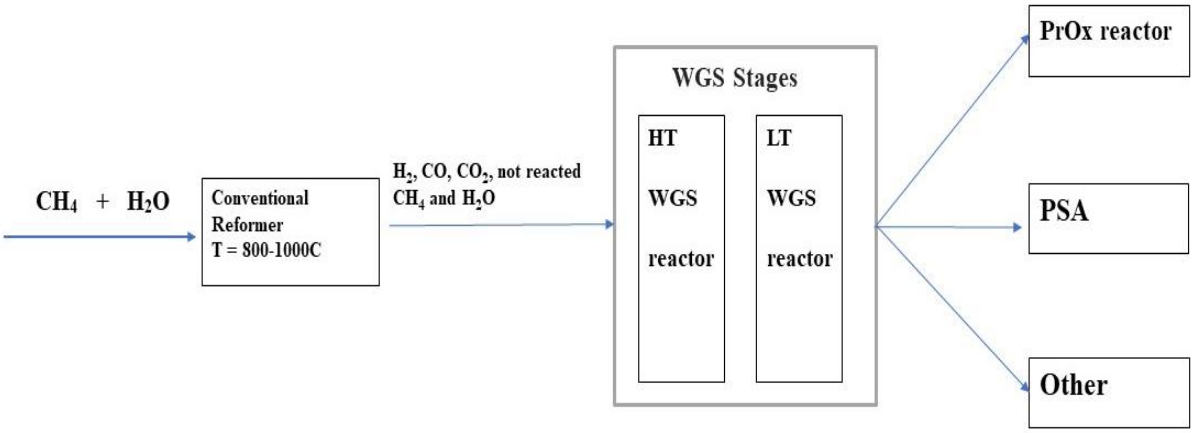

Fig 2.5 The scheme of high-grade hydrogen production via SRM reaction[45]

Carbon capturing and storage (CCS) is a method directed in conventional steam reforming and autothermal reforming. This is a very convenient process for tackling the very alarming situation of climate change [45]. The idea is very simple, the CO_2 has been captured at outlet points where it is dispatched to the atmosphere. Although, the idea has its complications. This is suitable for large scale operation units. On a smaller scale such as in the transportation sector, the cost of operation makes it suitable for reliable operations. Therefore, this process is good for power plants and high scale industries [46].

To synthesize a proper catalyst, a metal is spread over the support to avoid catalyst sintering and to reduce carbon formation [47]. The role of the catalyst is very important in SRM because coke formation during the process is the major issue which consequently deactivates the catalyst performance. Some noble metals for instance Pt, Ru, and Rh turned out to be efficient catalysts since these metals show high reactivity and less carbon deposition. So, their rare availability and high cost are not feasible for usage [48]. Nickel-based catalysts are widely used on an industrial scale. But, it takes a higher steam: methane molar ratio from 3 to 3.5 for proper gasification and to avoid coke formation [47]. On the other hand, cobalt is a good selection because it is not expensive as noble metal and is readily available. More interestingly, it has a good performance of reactivity and produces a rich synthetic gas (H_2 and CO) of near ratio to unity[49].

2.6 Catalysis in steam reforming of methane and the role of catalyst support

Typically to develop an active and stable catalyst for reforming techniques is the major deal. Generally, the catalysts of methane reforming consist of transition metal dispersed over catalyst support preferably high surface area of more than 100 m^2/g. The high surface area produces more product molecules in this way. It is very important to prepare well crystalline microstructures thus it must act as an active part of catalysis [50, 51]. Simankov et al [51] studied the mechanism of combined SRM and WGS process mechanism by using density functional theory (DFT). In the process of SRM, the CH_4 and H_2O or CO_2 are initially adsorbed at the surface of the catalyst and then desorbs as the final product. Fig 2.6 epresents the schematic of combined SRM and WGS system. Where the elementary steps of process are represented in Eqs.(8).

$$CH_4 + 2^* \rightleftharpoons CH_3^* + H^*$$

$$CH_3^* + {}^* \rightleftharpoons CH_2^* + H^*$$

$$CH_2^* + {}^* \rightleftharpoons CH^* + H^*$$

$$CH^* + {}^* \rightleftharpoons C^* + H^*$$

$$H_2O + 2^* \rightleftharpoons OH^* + H^*$$

$$OH^* + {}^* \rightleftharpoons O^* + H^*$$

$$2H^* \rightleftharpoons H_2 + 2^* \qquad (8)$$

$$C^* + O^* \rightleftharpoons CO^*$$

$$CO^* \rightleftharpoons CO + {}^*$$

$$CO^* + OH^* \rightleftharpoons HCOO^* + {}^*$$

$$HCOO^{*} \rightleftharpoons CO_2 + H^{*}$$

$$CO^{*} + O^{*} \rightleftharpoons CO_2 + 2^{*}$$

The dissociation of CH_4 requires a metallic surface whereas, the H_2O dissociation can also occur on support surface if the surface supports the redox reactions.

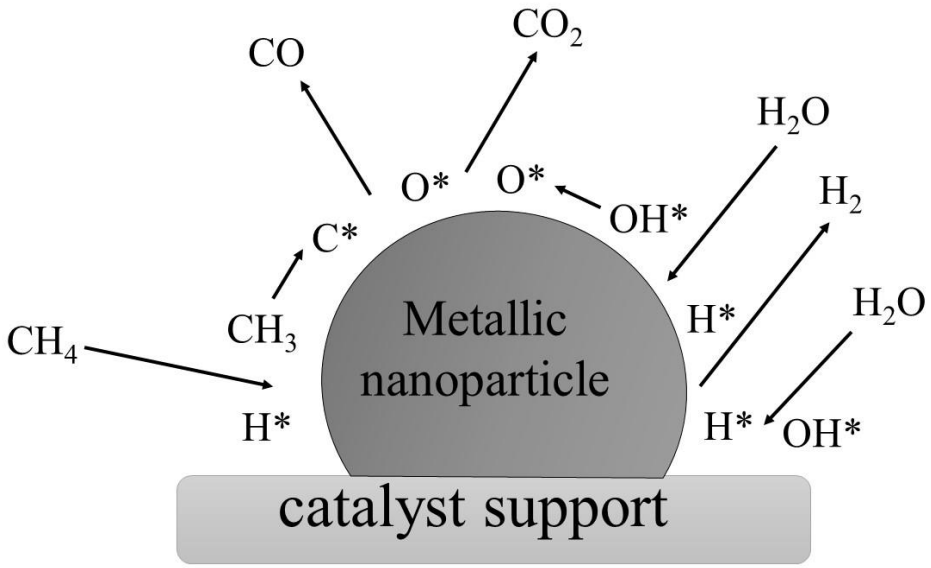

Fig 2.6 The schematic representation of the SRM-WGS process occurring at catalyst support

2.7 Active metal

The catalytic activity of the catalyst is correlated with a metal surface area which is the number of active sites. The good dispersion of active sites over the large surface area benefits the catalytic activity. Practically, the dispersion of catalysts is maintained to 2-5wt% with a size particle of 20-50nm. The higher than 15-20wt% usually does not produce the active sites resulting not better activity [50]. The structure of active metal over the surface area is also one of the major factors that define the catalytic activity apart from the active sites. For instance, the closed packed surface of Ni (111) has less efficient results than the (110) open packed Ni surface. It is also noticed that the lattice distortion also plays a critical role in catalytic activity.

Noble metals such as Platinum (Pt), Rhodium (Rh), Palladium (Pd), and Ruthenium (Ru) are regarded as the best active metals for catalytic activity [52]. Ni and Co are most used as active metals as compared to noble metals because of their low cost and readily available. The coke formation is the main issue that hampers their extensive use. There are some new techniques such as making alloys with noble metals and other bi-metal techniques that improve their stability and resistance towards the coke formation [53].

2.8 Catalyst Support

Catalyst support generates the catalytic active centres for the supported metals. The activity of support materials is highly governed by their chemical properties such as chemical stability and some physical properties. Moreover, some other factors such as surface area and disposal of metal particles over the surface play an important role [54]. Primarily, an expensive or rare catalyst is spread over large support to enhance its use and to increase the mechanical properties. The catalytic active sites become more stable when they are deposited on the micro pores of the support. When a suitable interaction between active sites and surface supports is carried out, it not only increases the concentration of active sites but also passes through maximum concentration [55]. Catalyst supports generates the catalytic active sites for supported metal. The functioning catalyst support material has greater surface area which is used to disperse the metal particles over the surface, at the same time shows chemical stability as well. The chemical and physical properties of materials surface define the effect of activation by generating the characteristic properties over the supported metal particles. Hence, under these ideas a lot of oxides and carbon material are better choice for catalyst support. For example, a well-known neutral material such as SiO_2 serves as a better catalyst support [6].

For designing heterogeneous catalysts, the porous carbon materials are a good candidate for developing catalyst support. The physical and chemical properties are used to generate a large surface area for better dispersion of active phases, and the pore size distribution is also monitored, which governs the diffusion of reactants and products to and from the surface [56]. The expensive catalysts are spread over the support to maximize the surface area and it also increases the mechanical properties of catalysts.

2.9 Activated Carbon as Catalyst Support

Activated carbon naturally exhibits amorphous behaviour that is good for developing porous structures and large internal surface area, and is also a reasonable cheap absorbent [57]. The choice of activated carbon as catalyst support has several advantages. It is inert in acidic and basic conditions and does not show reactivity. Another benefit is, concerning the applied application, the porous size and chemical properties of active sites on the surface can be adjusted accordingly. The metal particles can be retrieved by burning the catalyst support, which is why it is widely used for developing heterogeneous catalysts [58]. Carbon is a considerably attractive material for chemical and enzymatic transformations because of its high surface area and porosity, electrons conductivity, and its inertness. Carbon can be used for developing improved novel catalytic activity. The metallic nanoparticles (NPs) are impregnated on the surface by a chemically functionalization/decoration process. Because of these porous properties, carbon materials as a support are effectively good for heterogeneous catalysis as compared to oxide supports. The oxide supports such as TiO2, γ-Al2O3, hydrotalcite, and mesoporous silica, are unstable at high temperature and pressures, particularly in pressurized water reactions, which is utilized in the biomass transformation process [59].

Biomass includes lignocellulose which consists of cellulose, hemicellulose, lignin and a little number of inorganic materials. The primary resources are sugar crops, starch crops and aquatic plants. It also includes the wastes and residues from agriculture, forests, used plant oils, animal fats and municipal sites. In dry wood, there is around 40-45% is cellulose. Cellulose is a linear polymer of D-glucopyranose units which is linked by B-1-4 glycosidic bonds with crystalline and amorphous domains. About 25-35% of dry wood is hemicellulose which is a branched polysaccharide. The rest part is mostly lignin, which is a complex-amorphous polymer of varying phenyl propane units bridged by ether and carbon-carbon bonds. Fuel alcohols and other chemicals are produced from glucose monomers which can be obtained by hydrolysis of cellulose. Hemicellulose is a major feedstock for the production of furfural and derivates whereas lignin is a potential feedstock for high-value fuels [60] (lignin-derived, Mathew lingholtz). Lignocellulosic carbon materials are major feedstock for the production of activated

carbons [61]. These conversions are not so viable economically, however, the discovery of new shale gas reserves decreased the financial pressure [62].

2.10 Activated Carbon-based Materials for steam reforming techniques

The role of support is vital in catalyst synthesis since it decides the activity and deactivation of the catalyst [63-65]. Catalyst support generates the catalytic active centres for the supported metals. The activity of support materials is highly governed by their chemical properties such as chemical stability and some physical properties. Moreover, some other factors such as surface area and disposal of metal particles over the surface play an important role [54]. Primarily, an expensive or rare catalyst is spread over large support to enhance its use and to increase the mechanical properties. The catalytic active sites become more stable when they are deposited on the micropores of the support. When a suitable interaction between active sites and surface supports is carried out, it not only increases the concentration of active sites but also passes through maximum concentration [59]. The carbon materials as catalyst support have been used in heterogeneous catalysts for the last two decades [66, 67]. The activated carbon has more scope in this regard because it has various advantages when used as catalyst support. For example, low cost made them readily available, good mechanical resistance, modifying pore size upon requirement, and recovery of metal from spent catalyst [68].

AC is widely used in various applications such as catalysts themselves and catalyst supports [69-72], wastewater treatments [73], adsorbent [74], storage materials [75], and supercapacitor applications [76-79]. *Bubanale et al. (2017)* studied in detail the applications of AC from the very beginning ages. It had been used for pharmaceutical purposes at the very beginning times. Then with the industrial revolution, AC carbon was widely used for decolourization purposes in chemical industries [80].

2.11 Precursor Material for activated carbon

While preparation of activated carbon, the raw and cheap material with greater carbon content has been selected. The organic and inorganic material both are chosen as a precursor for activated carbon synthesis, whereas, some ionic liquid solutions and deep eutectic solution are used as special precursors while preparing activated carbon. The chemical and physical

properties are highly dependent on the precursor material selected and the way of preparation and activation method are also one of the influencing factors of characteristic properties of activated carbon [81]. The choice of agricultural waste for activated carbon is rather attractive for the researcher. The animal, forest and agriculture waste is overwhelmingly chosen as a material precursor for activated carbon synthesis since these are cheap raw materials readily available. Table 2.2 represents some agricultural wastes that are extensively utilized while activated carbon preparation with proximate and ultimate analysis [82].

Table 2.2 Proximate and ultimate analysis for agricultural residues

Agricultural waste	Proximate analysis (% w/w)			Ultimate analysis (% w/w)				
	Moisture	**Ash**	**Volatiles**	**C**	**H**	**N**	**S**	**O**
Palm shell	7.96	1.10	72.47	50.01	6.9	1.9	0.0	41
Palm stem	6.06	4.02	72.39	45.56	5.91	0.82	–	47.71
Grape stalk	15.69	10.16	51.08	46.14	5.74	0.37	0.0	36.60
Bamboo	–	3.90	80.6	43.8	6.6	0.4	0.0	–
Coconut shell	8.21	0.1	73.09	48.63	6.51	0.14	0.08	44.64
Olive mill	<5.0	<1.0	–	45.64	6.31	1.42	–	–
Almond shell	10.00	0.60	80.30	50.50	6.60	0.20	0.01	42.69
Wallnut shell	11.00	1.30	71.80	45.10	6.0	0.3	0.0	48.60
Almond tree pruning	10.60	1.20	72.20	51.30	6.50	0.80	0.04	41.36
Olive stone	10.40	1.40	74.40	44.80	6.0	0.1	0.01	49.09
Bamboo	2.44	6.51	69.63	45.53	4.61	0.22	–	–
Durian shell	11.27	4.84	–	39.30	5.90	1.00	0.06	53.74
Chinese fir sawdust	4.88	0.32	79.92	48.95	6.54	0.11	0.00	39.20
Banana empty fruit bunch	5.21	15.73	78.83	41.75	5.10	1.23	0.18	51.73

***Delonix regia* fruit pods**	0.22	2.80	92.03	34.22	4.50	1.94	0.42	58.91
Corn cob	4.3	0.90	78.7	46.8	6.0	0.9	–	46.3
Pomegranate seed	5.38	1.83	78.71	49.65	7.54	4.03	0.65	38.13
Birch	4.4	0.18	–	48.4	5.6	0.2	–	45.8
Salix	7.3	0.75	–	48.8	6.2	1.0	–	43.4
Sugarcane bagasse	6.2	0.90	–	47.3	6.2	0.3	–	46.2
Wheat straw	3.3	3.23	–	46.5	6.3	0.9	–	46.3
Bagasse	–	6.2	83.3	41.55	5.55	0.03	–	52.86
Rice husk	–	16.7	67.5	36.52	4.82	0.86	–	41.10
Cassava peel	11.4	0.3	59.4	59.31	9.78	2.06	0.11	28.74
Rice stalk	14.17	14.93	66.33	40.79	7.66	1.17	0.49	49.89
Woody birch	6.6	0.2	81.2	48.4	5.6	0.2	–	45.8

2.12 Activated carbon preparation

The activated carbon (AC) is either prepared through direct activation of raw material or gone through a two-step process that is the carbonization of material first then activation operation is carried out. In carbonization, the hydrocarbons are evaporated in distilled apparatus at a temperature less than 700 ℃ in an inert atmosphere. The process is known to be pyrolysis and the product obtained in the result is referred to as char, biochar and carbonized material [83].

The next step is the activation of biochar. The variety of methods is being employed to activate the biochar. Alongside the well-known activation methods; the physical and chemical activation method, some other emerging methods are also utilized such as salt tempting and ultrasonic pyrolysis. The selection of specific activation methods primarily relies on the carbon source, the preparation process as well as the pre-treatment steps that are required prior to pyrolysis and activation of the precursor material [8].

2.12.1 Physical Activation

In the physical activation of biochar, there are two steps are being followed. The biochar is subjected to oxidizing gases typically CO_2 and steam and sometimes a mixture of gases at an evaluated temperature of 800 °C -1000 °C thus creating porous and high surface carbonaceous material through reactions (7-9).

$$C + O_2 \rightarrow CO_2 \qquad (9)$$

$$C + CO_2 \rightarrow 2CO \qquad (10)$$

$$C + H_2O \rightarrow CO_2 + 2H_2 \qquad (11)$$

There are several advantages and disadvantages of physical activation. The good thing about the physical activation is that it is a lower-cost operation and not much chemical waste has been observed. At the same time, the longer time of activation and bigger energy consumption are the drawbacks of physical activation [84].

2.12.2 Chemical Activation

Chemical activation of biochar is called a wet oxidation process which is in step-process. The chemical activation is typically suitable for high cellulosic materials such as wood and fruit pits [82]. During the chemical activation process, the organic material is treated with chemical agents at high temperatures. The chemical agents are typically strong oxidants and dehydrate such as KOH, $ZnCl_2$, H_3PO_4, K_2CO_3, etc. Sequentially, the carbonaceous material is impregnated with chemical agents and activated simultaneously giving better porosity. Relatively to physical activation, the chemical activation requires less energy, a limited period, much better porosity and high surface area. Table 2.3 represents the activated carbon achieved from various precursor materials by the chemical activation method [83].

Table 2.3 Different types of activated carbon obtained by chemical activation method

Precursor	**Types of reagents**	**BET surface area (m_2/g)**	**Pore volume (m_3/g)**	**AC yield (%)**
Commercial AC	H_2SO_4	605	0.75	-
Orange peels	K_2CO_3	1104.45	0.615	80.9
Pineapple peels	K_2CO_3	680	0.45	-
Walnut shell	H_3PO_4	789	0.304	80
Coconut residue	H_3PO_4	58	0.025	93.31
Date palm pits	H_3PO_4	952	1.380	41
Cotton cake	H_3PO_4	584	0.298	29.8
Walnut shells	H_3PO_4	668	0.64	-
Wood-plastic composite waste	H_3PO_4	1711.27	0.863	-
Pineapple peels	KOH	1006	0.59	-
Petroleum coke	KOH	2940	1.658	47.95
Oil palm empty fruit bunch	KOH	1141	0.6	17.96
Date press cake	KOH	2632.5	1.239	44.5
Tamarind wood	$ZnCl_2$	1322	1.042	45.26
Tomato processing solid waste	$ZnCl_2$	1093	1.569	38.20
Date stones	$ZnCl_2$	1045	0.641	40.4
Cotton stalks	$ZnCl_2$	794.84	0.63	37.9

Cashew nutshell	$ZnCl_2$	1100	0.565	59
Date press cake	NaOH	2025.9	0.932	26.2
Coconut shell	NaOH	2825	1.498	18.8
Macadamia nut shells	NaOH	1524	0.826	19.79

In the light acid-basic theory of the chemical activation process, the chemical agents are categorized into further four groups such as acidic, alkaline, neutral, and self-activating agents. These chemical agents take a variety of biomass having cellulose, hemicellulose, lignin, and polysaccharides leading to a specific mechanism of activation. The porous structures develop in activated carbon through the synergetic effect of pore expansion, pore formation, pore combination and pore collapse [85].

2.13 Kinetics in steam reforming

The activation of methane (CH_4) is the rate-limiting step in the kinetics of steam reforming of methane. The activation of CH_4 happens by collision phenomenon, where CH_4 dissociates into CH_3 and H species. The H atoms in CH_3 have high energy, which can cause carbon formation. The direct rate of steam reforming of methane is pseudo-first-order relation concerning partial pressure (p_{CH_4}).

$$r_d = k \times p_{CH_4} \tag{12}$$

The turnover frequency (TOF) is calculated in this kinetic model, that would be the function of temperature (T) and partial pressures (P_x).

$$TOF(T, P_x) = 2 \times P_{CH_4} \times \theta^{*^2} \left(\vartheta . e^{\left(\frac{-E_B}{K_B . T} \right)} \right) \left(1 - \frac{P_{CO} \bullet P^3 H_2}{K_{eq} \bullet P_{CH_4} \bullet P_{H_2O}} \right) \tag{13}$$

$$TOF(T,P_x) = 2 \times k \times P_{CH_4} \times \theta^{*^2} \left(1 - r\right) \quad (14)$$

$$r = \left(1 - \frac{P_{CO} \bullet P^3 H_2}{K_{eq} \bullet P_{CH_4} \bullet P_{H_2O}}\right) \quad (15)$$

The parameter θ* is the empty sites, whereby CH_4 collides. E_a denotes the activation energy, whereas the K_B represents a Boltzmann's constant, T represents the temperature and ϑ denotes the pre-exponential factor. Khomenko et al. calculated the kinetics of steam reforming of methane by using a quasi-steady state in terms of the Temkin identity at a temperature range of 470-700 °C.

$$r = \frac{k \times P_{CH_4} \times P_{H_2O} \times r}{f\left(P_{H_2O}, P_{H2}\right)\left(1 + \frac{K_{H_2O} \bullet P_{H_2O}}{P_{H_2}}\right)} \quad (16)$$

Where k is constant, K_{eq} is the equilibrium constant and $f(P_{H_2O}, P_{H_2})$ is the polynomial factor in terms of P_{H_2O} and P_{H_2}.

The performance of the catalyst is determined by the methane conversion, which is compared with theoretical thermodynamic equilibrium. The sampled gas is fed into GC (Gas chromatography), which detects the gases such as CH_4, H_2, CO, and N_2 by using the TCD (Thermal conductivity detector). The conversion of CH_4 and the selectivity of H_2 and CO is given in the following equation [86].

Conversion:

$$CH_4(\%) = \frac{moles\,of\ CH_4\ converted}{moles\,of\ CH_4\ Introduced} \times 100 \quad (17)$$

Selectivity:

$$H_2(\%) = \frac{moles\,of\ H_2\ produced}{2 \times moles\,of\ CH_4\ converted} \times 100 \text{ [87, 88]} \quad (18)$$

$$CO(\%) = \frac{moles\ of\ CO\ produced}{[moles\ of\ CH4 + moles\ of\ CO2]converted} \times 100 \quad (19)$$

The conversion of methane is calculated as follows:

$$X_{CH_4}, \% = \left(1 - \frac{[CH_4]_{out}}{\alpha \times \left([CH_4]_{out} + [CO_2]_{out}\right)}\right) \times 100 \quad (20)$$

Where α is the methane content in the fuel. For pure methane, it is 1.

The yield of Hydrogen[89, 90]:

$$Y_{H_2}, \% = \frac{moles\ of\ H_2\ produced}{4 \times moles\ of\ CH_4\ Introduced} \times 100 \quad (21)$$

The surface rate of methane consumption is the rate of methane consumed per surface of active metal:

$$r_{CH_4} = \frac{X_{CH_4} \times F_{CH_4 in}}{SSA_{metal} \times m_{cat}} \quad (22)$$

where $X_{CH_4}$is the conversion of methane, $F_{CH_{4,in}}$is the molar flow rate of methane into the reactor, SSA_{metal} is the specific surface area of metal and m_{cat} is the mass of loaded catalyst.

$$Deactivation, \% = \left(\frac{X_o - X_t}{X_o}\right) \times 100 \quad (23)$$

The long-term stability test has been carried out for the deactivation of the catalyst, which is the conversion of methane at the start of the reaction (X_0) with time t (X_t).

There are enormous studies redeemed to investigate the kinetics involve in steam reforming. Ki-Dong Ko et al. [91] investigated the kinetics of SRM by using the Marquardt method reaction. According to the study, the reaction rate step becomes more complicated if adsorption and desorption include on the catalyst surface. Conveniently, simple power-law

equation Eq. (24) is more feasible to use if product gases do not affect reaction rate.

$$r = k\ P_{CH_4}^{m}\ P_{H_2O}^{n} \tag{24}$$

This is generally accepted that the reaction rate equation is first order concerning methane. However, in some pieces of literature, the reaction order varies from zero to minus.

2.14 Thermodynamics in steam reforming

By far, a lot of studies have been carried out on various experimental and theoretical aspects of steam methane reforming. Tabrizi et al [92] studied the thermodynamics of SMR based Gibbs free energy minimization, and statistical methodology. According to their investigation, they have studied the effects of different parameters such as temperature, pressure, and the ratio of feedstock, and more importantly, their interactions have been investigated. Which were not discussed in previous studies mainly on the statistical methodology approach [92].

Gibb's free energy minimization gives the composition of complicated chemical reactions [93]. In the equilibrium configuration, the system is thermodynamically favourable when the system has minimal energy, which means mathematically the differential of a system must be zero at a given temperature and pressure [94].

$$\left(dG^{t}\right)_{T,p} = 0 \tag{25}$$

The Gibbs free energy of a chemical reaction is as given in Eq. (26):

$$G^{t} = \sum_{i-1}^{N} n_i \mu_i \tag{26}$$

$$\mu i = \Delta G_{f_i}^{o} + RT \ln\left(\hat{f}\ /\ f_i^{o}\right) \tag{27}$$

The parameter G^{t} is the total Gibbs free energy at constant temperature and pressure. N represents the number of species in the feedstock and in is the number of moles of species.

Eq.(27) is the chemical potential equation. $\hat{f}$ represents the fugacity in the system and f_i^{o} is the standard fugacity.

$$\hat{f}_i = y_i \hat{\phi}_i P \tag{28}$$

$$f_i^o = P_o \tag{29}$$

Where y_i represents the molar fraction of species *i* and $\hat{\phi}$ represents the fugacity coefficient of species *i* in the feedstock.

$$\sum_i^N n_i \left(\Delta G_{fi}^o + RT \ln\left(\hat{f}_i / f_i^o \right) + \sum_k \lambda_i a_{ik} \right) = 0 \tag{30}$$

Eq. (30) becomes when Lagrange multipliers are introduced in gas phase equilibrium conditions. The parameter ΔG_{fi}^o is the standard Gibbs free energy formation, R is the universal gas constant.

$$\sum_i^{N-1} n_i \left(\Delta G_{fi}^o + RT \ln\left(\hat{f}_i / f_i^o \right) + \sum_k \lambda_i a_{ik} \right) + \left(n_c \Delta G_{fc(s)}^o \right) = 0 \tag{31}$$

Eq. (31) is the final equation. The Gibbs free energy and enthalpy of different species are in Table 2.4. To calculate coke formation, graphite is presented, which has zero Gibbs free energy and is calculated only in elemental constraints.

Table 2.4 The list of the number of Gibbs free energy and enthalpy of formation

Species	$\Delta H_{298}^o (kJ/mol)$	$\Delta G_{298}^o (kJ/mol)$
CH_4	-74.5	-50.5
CO	-110.5	-137.2
CO_2	-393.5	-394.4
H_2	0	0
H_2O	-241.8	-228.6
O_2	0	0
C	0	0

The mathematical relation of SMR among temperature, pressure and inlet steam per methane is determined by the second-order polynomial equation, which is given in Eq. (32) :

$$Y = B_o + \sum_{i=1}^n B_i x_i + \sum B_{ij} x_i x_j + \sum_{j=1}^n B_{jj} x_j^2 \tag{32}$$

In Eq. (32), Y is the response of dependent variables, whereas B is the regression coefficient, and x is the test variables. The test variable model equation is given in Eq. (33) :

$$x_i = \frac{X_i - X_i^*}{\Delta X_i} \tag{33}$$

The parameter x_i is the coded value and X_i is the encoded value of the *i*th independent variable, whereas X_i^* is the encoded value of the *i* th independent variable. ΔX_i is the step change value.

The primary gases which are formed in SMR experiments are H_2, CO, CO_2, H_2O, and CH_4. In SMR reaction, the water-gas-shift reaction is sparsely exothermic, which comes along at very low temperatures. Whereas the reverse water-gas-shift is highly endothermic and occurs at high temperatures.

The reactions of the equilibrium conversions of reactants and the yield of products[95] and the H_2/CO ratio[96] are given as:

$$CH_4\ conversion\,(\%) = \frac{[CH_4]_{in} - [CH_4]_{out}}{[CH_4]} \times 100 \tag{34}$$

$$H_2O\ conversion\,(\%) = \frac{[H_2O]_{in} - [H_2O]_{out}}{[H_2O]_{in}} \times 100 \tag{35}$$

$$CO\ yield\ (\%) = \frac{[CO]_{out}}{[CO_2]_{in} + [CH_4]_{in}} \times 100 \tag{36}$$

$$H_2\ yield\ (\%) = \frac{2 \times [H_2]_{out}}{4 \times [CH_4]_{in} + 2 \times [H_2O]_{in}} \times 100 \tag{37}$$

$$H_2 / CO\ ratio = \frac{moles\ of\ H_2\ produced}{moles\ of\ CO\ produced} \tag{38}$$

Coke formation is the major issue that occurs at high temperatures. Although there are certain methods employed to avoid coke formation. For instance, by regulating the operation conditions of steam to carbon ratio and fuel to oxidant ratio. When the oxygen to carbon ratio is kept greater than 1, that prevents carbon formation because there is enough oxygen to oxidize. The deactivation of the catalyst after hours long of reactions is as follow:

$$\%D = \frac{XCH_4^{initial} - XCH_4^{hours}}{XCH_4^{initial}} \tag{39}$$

Where $XCH_4^{initial}$ and XCH_4^{hours} are the methane conversion factors at initial timings and after hours of running, respectively[96]

References

1. Grubler, A., et al., *A low energy demand scenario for meeting the 1.5 C target and sustainable development goals without negative emission technologies.* Nature energy, 2018. **3**(6): p. 515-527.

2. Guo, S., et al., *A review on the utilization of hybrid renewable energy.* Renewable and Sustainable Energy Reviews, 2018. **91**: p. 1121-1147.

3. Abe, J.O., et al., *Hydrogen energy, economy and storage: review and recommendation.* International journal of hydrogen energy, 2019. **44**(29): p. 15072-15086.

4. Ren, J., et al., *Current research trends and perspectives on materials-based hydrogen storage solutions: a critical review.* International journal of hydrogen energy, 2017. **42**(1): p. 289-311.

5. Tarhan, C. and M.A. Çil, *A study on hydrogen, the clean energy of the future: Hydrogen storage methods.* Journal of Energy Storage, 2021. **40**: p. 102676.

6. Morkovkin, D.E., et al. *Formation of a national environmental strategy for the fuel and energy complex*. in *IOP Conference Series: Materials Science and Engineering*. 2019. IOP Publishing.

7. Zhang, J., J. Zheng, and W. Yang, *Green supercapacitor assisted photocatalytic fuel cell system for sustainable hydrogen production.* Chemical Engineering Journal, 2021. **403**: p. 126368.

8. Oznobikhina, L. and E. Pirunova. *Enterprises of the fuel and energy complex-the sphere of high risks and objects of increased industrial danger*. in *IOP Conference Series: Earth and Environmental Science*. 2021. IOP Publishing.

9. Kamran, M., M.R. Fazal, and M. Mudassar, *Towards empowerment of the renewable energy sector in Pakistan for sustainable energy evolution: SWOT analysis.* Renewable Energy, 2020. **146**: p. 543-558.

10. Waris, I. and I. Hameed, *Promoting environmentally sustainable consumption behavior: an empirical evaluation of purchase intention of energy-efficient appliances.* Energy Efficiency, 2020. **13**(8): p. 1653-1664.

11. Papadis, E. and G. Tsatsaronis, *Challenges in the decarbonization of the energy sector.* Energy, 2020: p. 118025.

12. Meisel, K., et al., *Future renewable fuel mixes in transport in Germany under red ii and climate protection targets.* Energies, 2020. **13**(7): p. 1712.

13. Gao, N., et al., *Syngas production via combined dry and steam reforming of methane over Ni-Ce/ZSM-5 catalyst.* Fuel, 2020. **273**: p. 117702.

14. Boyano, A., et al., *Conventional and advanced exergoenvironmental analysis of a steam methane reforming reactor for hydrogen production.* Journal of Cleaner Production, 2012. **20**(1): p. 152-160.

15. Hanif, I., et al., *Fossil fuels, foreign direct investment, and economic growth have triggered CO2 emissions in emerging Asian economies: some empirical evidence.* Energy, 2019. **171**: p. 493-501.

16. Acar, C., I. Dincer, and G.F. Naterer, *Clean hydrogen and power from impure water.* Journal of Power Sources, 2016. **331**: p. 189-197.

17. Gani, A., *Fossil fuel energy and environmental performance in an extended STIRPAT model.* Journal of Cleaner Production, 2021. **297**: p. 126526.

18. Capurso, T., et al., *Perspective of the role of hydrogen in the 21st century energy transition.* Energy Conversion and Management, 2022. **251**: p. 114898.

19. Jain, I., *Hydrogen the fuel for 21st century.* International journal of hydrogen energy, 2009. **34**(17): p. 7368-7378.

20. Acar, C. and I. Dincer, *The potential role of hydrogen as a sustainable transportation fuel to combat global warming.* International Journal of Hydrogen Energy, 2020. **45**(5): p. 3396-3406.

21. Bartels, J.R., M.B. Pate, and N.K. Olson, *An economic survey of hydrogen production from conventional and alternative energy sources.* International journal of hydrogen energy, 2010. **35**(16): p. 8371-8384.

22. Zerta, M., et al., *Alternative World Energy Outlook (AWEO) and the role of hydrogen in a changing energy landscape.* International journal of hydrogen energy, 2008. **33**(12): p. 3021-3025.

23. Maggio, G., A. Nicita, and G. Squadrito, *How the hydrogen production from RES could change energy and fuel markets: A review of recent literature.* International Journal of Hydrogen Energy, 2019. **44**(23): p. 11371-11384.

24. Abbas, H.F. and W.W. Daud, *Hydrogen production by methane decomposition: a review.* International journal of hydrogen energy, 2010. **35**(3): p. 1160-1190.

25. Stankiewicz, A., *Energy matters: alternative sources and forms of energy for intensification of chemical and biochemical processes.* Chemical Engineering Research and Design, 2006. **84**(7): p. 511-521.

26. Safari, F. and I. Dincer, *A review and comparative evaluation of thermochemical water splitting cycles for hydrogen production.* Energy Conversion and Management, 2020. **205**: p. 112182.

27. Ji, M. and J. Wang, *Review and comparison of various hydrogen production methods based on costs and life cycle impact assessment indicators.* International Journal of Hydrogen Energy, 2021. **46**(78): p. 38612-38635.

28. Yang, X., S. Wang, and Y. He, *Review of catalytic reforming for hydrogen production in a membrane-assisted fluidized bed reactor.* Renewable and Sustainable Energy Reviews, 2022. **154**: p. 111832.

29. Pajak, M., et al., *A multiobjective optimization of a catalyst distribution in a methane/steam reforming reactor using a genetic algorithm.* International Journal of Hydrogen Energy, 2020.

30. Nabgan, W., et al., *Renewable hydrogen production from bio-oil derivative via catalytic steam reforming: An overview.* Renewable and Sustainable Energy Reviews, 2017. **79**: p. 347-357.

31. Abdalla, A.M., et al., *Hydrogen production, storage, transportation and key challenges with applications: A review.* Energy conversion and management, 2018. **165**: p. 602-627.

32. Minh, D.P., et al., *Hydrogen production from biogas reforming: An overview of steam reforming, dry reforming, dual reforming, and tri-reforming of methane.* Hydrogen Supply Chains, 2018: p. 111-166.

33. Navas-Anguita, Z., et al., *Revisiting the role of steam methane reforming with CO2 capture and storage for long-term hydrogen production.* Science of the total Environment, 2021. **771**: p. 145432.

34. Dawood, F., M. Anda, and G. Shafiullah, *Hydrogen production for energy: An overview.* International Journal of Hydrogen Energy, 2020. **45**(7): p. 3847-3869.

35. Howarth, R.W. and M.Z. Jacobson, *How green is blue hydrogen?* Energy Science & Engineering, 2021.

36. Pajak, M., et al., *A multiobjective optimization of a catalyst distribution in a methane/steam reforming reactor using a genetic algorithm.* international journal of hydrogen energy, 2021. **46**(38): p. 20183-20197.

37. Kaiwen, L., Y. Bin, and Z. Tao, *Economic analysis of hydrogen production from steam reforming process: A literature review.* Energy Sources, Part B: Economics, Planning, and Policy, 2018. **13**(2): p. 109-115.

38. Rapier, R. *Estimating The Carbon Footprint Of Hydrogen Production*. Jun 6, 2020,06:00pm EDT [cited 2020 Jun 6,].

39. Zhang, H., Z. Sun, and Y.H. Hu, *Steam reforming of methane: Current states of catalyst design and process upgrading.* Renewable and Sustainable Energy Reviews, 2021. **149**: p. 111330.

40. Boudjeloud, M., et al., *La-doped supported Ni catalysts for steam reforming of methane.* international journal of hydrogen energy, 2019. **44**(20): p. 9906-9913.

41. Shagdar, E., et al., *Process analysis of solar steam reforming of methane for producing low-carbon hydrogen.* RSC Advances, 2020. **10**(21): p. 12582-12597.

42. Taji, M., M. Farsi, and P. Keshavarz, *Real time optimization of steam reforming of methane in an industrial hydrogen plant.* International Journal of Hydrogen Energy, 2018. **43**(29): p. 13110-13121.

43. Noh, Y.S., K.-Y. Lee, and D.J. Moon, *Hydrogen production by steam reforming of methane over nickel based structured catalysts supported on calcium aluminate modified SiC.* International Journal of Hydrogen Energy, 2019. **44**(38): p. 21010-21019.

44. Park, H.-G., et al., *Bench-scale steam reforming of methane for hydrogen production.* Catalysts, 2019. **9**(7): p. 615.

45. Cormos, A.-M., et al., *Economic assessments of hydrogen production processes based on natural gas reforming with carbon capture.* Chem. Eng. Trans, 2018. **70**: p. 1231-1236.

46. Rydén, M. and A. Lyngfelt, *Using steam reforming to produce hydrogen with carbon dioxide capture by chemical-looping combustion.* International journal of hydrogen energy, 2006. **31**(10): p. 1271-1283.

47. Lucredio, A.F. and E.M. Assaf, *Cobalt catalysts prepared from hydrotalcite precursors and tested in methane steam reforming.* Journal of power sources, 2006. **159**(1): p. 667-672.

48. Zhang, Y., et al., *Steam reforming of methane over Ni/SiO2 catalyst with enhanced coke resistance at low steam to methane ratio.* Catalysis Today, 2015. **256**: p. 130-136.

49. Izhab, I., M. Asmadi, and N.A.S. Amin, *Methane dry reforming using oil palm shell activated carbon supported cobalt catalyst: Multi-response optimization.* International Journal of Hydrogen Energy, 2021. **46**(48): p. 24754-24767.

50. Van Beurden, P., *On the catalytic aspects of steam-methane reforming.* Energy Research Centre of the Netherlands (ECN), technical report I-04-003, 2004.

51. Simakov, D.S., et al., *Solar thermal catalytic reforming of natural gas: a review on chemistry, catalysis and system design.* Catalysis Science & Technology, 2015. **5**(4): p. 1991-2016.

52. Liu, J.A., *Kinetics, catalysis and mechanism of methane steam reforming.* WPI Chemical Engineering Department, 2006.

53. Aramouni, N.A.K., et al., *Catalyst design for dry reforming of methane: Analysis review.* Renewable and Sustainable Energy Reviews, 2018. **82**: p. 2570-2585.

54. Sakata, Y., et al., *Preparation of a new type of CaSiO3 with high surface area and property as a catalyst support*, in *Studies in surface science and catalysis*. 2006, Elsevier. p. 331-338.

55. Jüntgen, H., *Activated carbon as catalyst support: a review of new research results.* Fuel, 1986. **65**(10): p. 1436-1446.

56. Marsh, H. and F. Rodriguez-Reinoso, *Sciences of carbon materials.* 2000.

57. Alhamed, Y.A., *Activated carbon from dates' stone by ZnCl2 activation.* JKAU Eng Sci, 2006. **17**(2): p. 5-100.

58. Iwanow, M., et al., *Activated carbon as catalyst support: precursors, preparation, modification and characterization.* Beilstein journal of organic chemistry, 2020. **16**(1): p. 1188-1202.

59. Matthiesen, J., et al., *Functional carbons and carbon nanohybrids for the catalytic conversion of biomass to renewable chemicals in the condensed phase.* Chinese Journal of Catalysis, 2014. **35**(6): p. 842-855.

60. Ahorsu, R., F. Medina, and M. Constantí, *Significance and challenges of biomass as a suitable feedstock for bioenergy and biochemical production: A review.* Energies, 2018. **11**(12): p. 3366.

61. Nabais, J.M.V., et al., *Production of activated carbons from almond shell.* Fuel Processing Technology, 2011. **92**(2): p. 234-240.

62. Dauenhauer, P.J. and G.W. Huber, *Biomass at the shale gas crossroads.* Green Chemistry, 2014. **16**(2): p. 382-383.

63. Tang, S., et al., *CO2 reforming of methane to synthesis gas over sol–gel-made Ni/γ-Al2O3 catalysts from organometallic precursors.* Journal of Catalysis, 2000. **194**(2): p. 424-430.

64. Matos, J., et al., *Methane Transformation in Presence of Carbon Dioxide on Activated Carbon Supported Nickel–calcium Catalysts.* Catalysis Letters, 2006. **109**.

65. Díaz, K., V. García, and J. Matos, *Activated carbon supported Ni–Ca: influence of reaction parameters on activity and stability of catalyst on methane reformation.* Fuel, 2007. **86**(9): p. 1337-1344.

66. Zhang, G., et al., *CO2 reforming of CH4 in coke oven gas to syngas over coal char catalyst.* Chemical Engineering Journal, 2010. **156**(3): p. 519-523.

67. Xu, L., et al., *Catalytic CH4 reforming with CO2 over activated carbon based catalysts.* Applied Catalysis A: General, 2014. **469**: p. 387-397.

68. Fidalgo, B., et al., *Synthesis of carbon-supported nickel catalysts for the dry reforming of CH4.* Fuel Processing Technology, 2010. **91**(7): p. 765-769.

69. Liew, R.K., et al., *Production of activated carbon as catalyst support by microwave pyrolysis of palm kernel shell: a comparative study of chemical versus physical activation.* Research on Chemical Intermediates, 2018. **44**(6): p. 3849-3865.

70. Lam, S.S., et al., *Activated carbon for catalyst support from microwave pyrolysis of orange peel.* Waste and Biomass Valorization, 2017. **8**(6): p. 2109-2119.

71. Dhelipan, M., et al., *Activated carbon from orange peels as supercapacitor electrode and catalyst support for oxygen reduction reaction in proton exchange membrane fuel cell.* Journal of Saudi Chemical Society, 2017. **21**(4): p. 487-494.

72. Galhardo, T.S., et al., *Glycerol valorization by base-free oxidation with air using platinum–nickel nanoparticles supported on activated carbon as catalyst prepared by a simple microwave polyol method.* Clean Technologies and Environmental Policy, 2018. **20**(9): p. 2075-2088.

73. Wong, S., et al., *Recent advances in applications of activated carbon from biowaste for wastewater treatment: a short review.* Journal of Cleaner Production, 2018. **175**: p. 361-375.

74. Saleem, J., et al., *Production and applications of activated carbons as adsorbents from olive stones.* Biomass conversion and biorefinery, 2019. **9**(4): p. 775-802.

75. Sevilla, M., A. Fuertes, and R. Mokaya, *Preparation and hydrogen storage capacity of highly porous activated carbon materials derived from polythiophene.* International journal of hydrogen energy, 2011. **36**(24): p. 15658-15663.

76. Han, X., et al., *A high performance nitrogen-doped porous activated carbon for supercapacitor derived from pueraria.* Journal of Alloys and Compounds, 2018. **744**: p. 544-551.

77. Misnon, I.I., N.K.M. Zain, and R. Jose, *Conversion of oil palm kernel shell biomass to activated carbon for supercapacitor electrode application.* Waste and Biomass Valorization, 2019. **10**(6): p. 1731-1740.

78. Cheng, F., et al., *Boosting the supercapacitor performances of activated carbon with carbon nanomaterials.* Journal of Power Sources, 2020. **450**: p. 227678.

79. Chen, D., et al., *Effect of Self-Doped Heteroatoms in Biomass-Derived Activated Carbon for Supercapacitor Applications.* ChemistrySelect, 2019. **4**(5): p. 1586-1595.

80. Bubanale, S. and M. Shivashankar, *History, method of production, structure and applications of activated carbon.* International Journal of Engineering and Technical Research, 2017. **6**: p. 495-498.

81. Munoz-Guillena, M., et al., *Activated carbons from Spanish coals. 1. Two-stage carbon dioxide activation.* Energy & fuels, 1992. **6**(1): p. 9-15.

82. Yahya, M.A., Z. Al-Qodah, and C.Z. Ngah, *Agricultural bio-waste materials as potential sustainable precursors used for activated carbon production: A review.* Renewable and Sustainable Energy Reviews, 2015. **46**: p. 218-235.

83. Heidarinejad, Z., et al., *Methods for preparation and activation of activated carbon: a review.* Environmental Chemistry Letters, 2020. **18**(2): p. 393-415.

84. Naji, S.Z. and C.T. Tye, *A review of the synthesis of activated carbon for biodiesel production: Precursor, preparation, and modification.* Energy Conversion and Management: X, 2022. **13**: p. 100152.

85. Gao, Y., et al., *Insight into activated carbon from different kinds of chemical activating agents: A review.* Science of the Total Environment, 2020. **746**: p. 141094.

86. Abbas, S.Z., V. Dupont, and T. Mahmud, *Kinetics study and modelling of steam methane reforming process over a NiO/Al2O3 catalyst in an adiabatic packed bed reactor.* International journal of hydrogen Energy, 2017. **42**(5): p. 2889-2903.

87. Palmer, C., et al., *Dry reforming of methane catalysed by molten metal alloys.* Nature Catalysis, 2020. **3**(1): p. 83-89.

88. Hao, Z., et al., *Characterization of aerogel Ni/Al2O3 catalysts and investigation on their stability for CH4-CO2 reforming in a fluidized bed.* Fuel Processing Technology, 2009. **90**(1): p. 113-121.

89. Wu, H.-C., Z. Rui, and J.Y. Lin, *Hydrogen production with carbon dioxide capture by dual-phase ceramic-carbonate membrane reactor via steam reforming of methane.* Journal of Membrane Science, 2020. **598**: p. 117780.

90. Meloni, E., et al., *Ultracompact methane steam reforming reactor based on microwaves susceptible structured catalysts for distributed hydrogen production.* International Journal of Hydrogen Energy, 2021. **46**(26): p. 13729-13747.

91. Ko, K.-D., et al., *Kinetics of steam reforming over a Ni/alumina catalyst.* Korean Journal of Chemical Engineering, 1995. **12**(4): p. 478-480.

92. Tabrizi, F.F., S.A.H.S. Mousavi, and H. Atashi, *Thermodynamic analysis of steam reforming of methane with statistical approaches.* Energy conversion and management, 2015. **103**: p. 1065-1077.

93. Li, Y., et al., *Thermodynamic analysis of autothermal steam and CO2 reforming of methane.* International Journal of Hydrogen Energy, 2008. **33**(10): p. 2507-2514.

94. Aktaş, S., M. Karakaya, and A.K. Avcı, *Thermodynamic analysis of steam assisted conversions of bio-oil components to synthesis gas.* International Journal of Hydrogen Energy, 2009. **34**(4): p. 1752-1759.

95. Özkara-Aydınoğlu, Ş., *Thermodynamic equilibrium analysis of combined carbon dioxide reforming with steam reforming of methane to synthesis gas.* international journal of hydrogen energy, 2010. **35**(23): p. 12821-12828.

96. Soria, M., et al., *Thermodynamic and experimental study of combined dry and steam reforming of methane on Ru/ZrO2-La2O3 catalyst at low temperature.* International Journal of hydrogen energy, 2011. **36**(23): p. 15212-15220.

Chapter 3

Methodology

3.1 Activated Carbon (AC) synthesis

The locally obtained hemp leaves are used as biomass precursors to synthesize an activated carbon (AC). The schematic of AC synthesis is represented in Fig. 3.1(a). Initially, the hemp leaves were undergone pre-treatment stages where hemp leaves were separated thoroughly cleaned and washed. Sequentially, the hemp leaves were properly dried in an oven at 80 °C and finally ground in mortar and pestle. For specific particle size, the ground hemp was sieved out at the size of 0.6 mm. In the carbonization, the biochar (BC) has been produced in a tube furnace (GSL-1800X, MTI corporation), heated at 750 °C for 2 h at a heating rate of 10 °C/min in an inert atmosphere with an N_2 gas flow of 40 ml min^{-1}. The yield of BC produced is calculated using Eq. (40).

$$Yield_{(BC)} = \frac{wt.of\ BC_{produced}}{wt.of\ Biomass} \times 100 \quad (40)$$

The obtained BC was activated with hydrogen peroxide H_2O_2 (30% purity) by mixing 1.0 g of BC to 10 ml H_2O_2 ratio under constant stirring of 6 h at room temperature. The modified material has been washed thoroughly with distilled water until effluent in colour, sequentially dried overnight at temperature of 110 °C in the electric oven, the resulting material is labelled as activated carbon (AC). Table 3.1 represents the elemental analysis of BC and AC as determined by the CHNS analyser (CKIC 5E-2200)[1].

Table 3.1 The elemental analysis BC and AC via CHNS analyser

Sample	**Carbon (%)**	**H_2 (%)**	**N_2 (%)**
BC	45.70	1.08	0
AC	43.26	1.12	0

3.2 Preparation of Ni-Co loaded AC catalyst

The chemicals and materials that are utilized for catalyst synthesis in the experiment were cobalt (II) nitrate $Co(NO_3)_2.6H_2O$ and nickel nitrate $Ni(NO_3)_2 \cdot 6H_2O$ (98% purity, Sigma Aldrich), hydrogen peroxide H_2O_2 (30% purity), and distilled water for washing purposes.

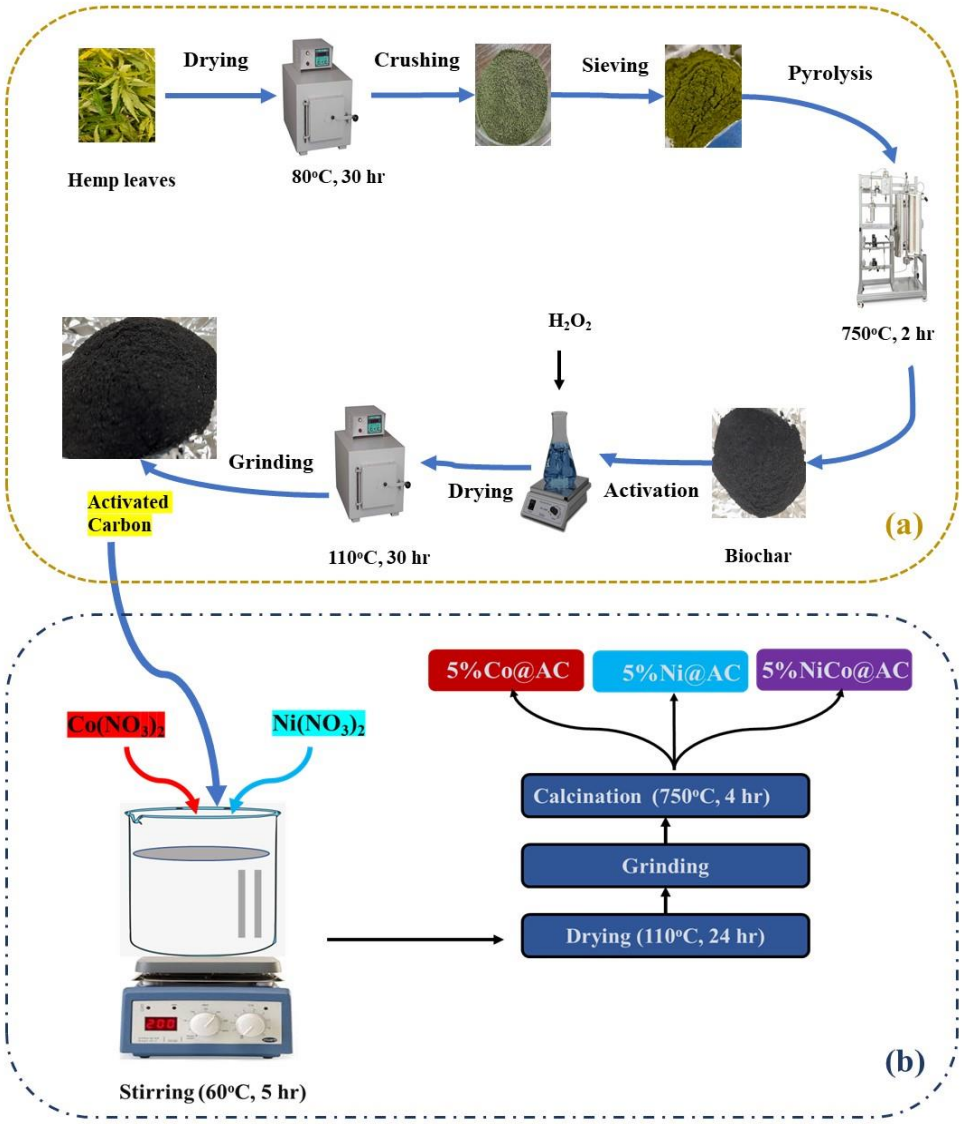

Fig 3.1 The schematic diagram of material synthesis (a) AC (b) 5%Co@AC, 5%Ni@AC and 5%NiCo@AC

The wetness impregnation method was used to prepare monometallic Ni, Co catalyst, and Ni-Co bimetallic catalysts with high activity and high distribution as represented in Fig. 3.1(b). The AC was used as catalyst support for catalyst preparation.

Cobalt nitrate ($Co(NO_3)_2.6H_2O$ and nickel nitrate $Ni(NO_3)_2 \cdot 6H_2O$ salts are used as an active metals for catalyst preparation. The AC was immersed in a solution of cobalt nitrate ($Co(NO_3)_2.6H_2O$ (0.04 M) and Nickel Nitrate $Ni(NO_3)_2 \cdot 6H_2O$ (0.04M) with constant stirring at 60 °C for 5 h. The monometallic Co and Ni catalysts were sequentially impregnated on catalyst support with impregnation rates of 5wt.% in terms of relative AC mass added. Following the same process, bimetallic Ni-Co catalyst is prepared by co-impregnation with 5wt.% impregnation rates. The resulting slurry was dried overnight at 110 °C in an electric oven. Sequentially, the dried material is ground to fine powder form. In the final stage, the material is passed through the calcination stage at a temperature of 750 °C for 4 h stay time in a tube furnace in an inert atmosphere to remove volatile impurities. The final resulted catalyst is named a 5%Co@AC, 5%Ni@AC, and 5%Ni-Co@AC catalysts.

3.3 Catalyst characterization

The various characterization techniques were employed to analyse the physicochemical and structural properties of synthesized and spent catalysts.

The XRD technique is used for phase composition and lattice symmetry by using Model dron8 Russia radiation source: copper kalpha. The operating conditions for XRD analysis are as follow; the 2θ measured from 20 °to 80° for fresh catalysts whereas for spent catalyst 2θ ranges from 5 to 90 at 0.05 step size, 30 min scan rate. The identification of the peaks of the calcined and ground samples was carried out via a Bruker D8 advanced X-ray diffractometer with an irradiation wavelength of 1.5418 Å at 40 kV and 20 mA testing conditions.

SEM is tested for morphology and texture of fresh and spent catalysts at different magnifications by using the JSM-6490A JEOL Japan machine with a resolution power of 3 nm at 30 kV with an extension of 10–200,000X. Whereas elemental analysis is performed at EDX (Z2-i7, analyser, EDAX Ametek) to investigate the elemental composition of a material.

The FTIR is analysed for specific functional and structural groups of all materials including powdered hemp leaves by using Cary 630 FTIR (Agilent Technologies) at wavenumber ranges

from 4000-650 cm^{-1}. The surface area, pore characteristics, and volume distribution of prepared catalyst and spent catalyst is calculated by N_2 adsorption-desorption BET theory (Quantachome Instruments version 11.05) analysis at 77.3 K bathing temperature. Before measurement, the samples were subjected to outgassing at a temperature of 300 °C for 10 h stay time in a vacuum to clean and dry the surface.

The TGA is performed by using TGA5500 (Discovery, series) for thermal stability and to determine the carbon deposition on spent catalyst by maintaining nitrogen flow of 100ml/min, heating ramp 20 °C/min up to 900 °C.

3.4 Experimental setup and catalytic activity for SMR

The experimental setup of SMR is shown in Fig 3.2. The SMR has been conducted in a thermal fixed bed reactor (Parr Instrument, 5401, USA), having stainless steel (SS 316) rod (14mm outer diameter and 12 mm inner diameter, length = 300 mm) with a single zone heating furnace. The CH_4 flow rate is monitored by a mass flow controller (Brooke instruments, USA), and the temperature of the reactor is regulated by the process controller (4871, Parr instrument) using a K-type thermocouple. The temperature and flow rates are controlled under the online SCADA system. The catalyst (0.30 g) has been placed in the centre of the SS rod, sandwiched between quartz wool to maintain a uniform temperature. The peristaltic pump provides the water at a flow rate of 20 ml/min and enters the preheater, and ten into the reactor along with CH_4 at the flow rate of 10 ml/min. Before the reaction, the sample was reduced under a hydrogen flow rate of 40 ml/min for 1h at a temperature of 750 °C. After the reduction, the temperature was maintained at 750 °C and introduced reactants. The reactant and product gases analysis were conducted in a gas chromatograph (GC 2010 plus, Shimadzu) equipped with a thermal conductivity detector (TCD). The TCD column details are reported elsewhere [2].

The performance of the catalyst is determined by the methane, H_2 and CO fractional development [3]. Eq. (41) represents the conversion of methane, whereas, Eq. (42) and (43) represents the selectivity of hydrogen and carbon monoxide respectively [4-9].

$$CH_4(\%) = \frac{CH_4\ converted}{CH_4\ Introduced} \times 100 \qquad (41)$$

$$H_2(\%) = \frac{H_2\ produced}{2 \times CH_4\ converted} \times 100 \tag{42}$$

$$CO(\%) = \frac{CO\ produced}{\left[CH_4 + CO_2\right] converted} \times 100 \tag{43}$$

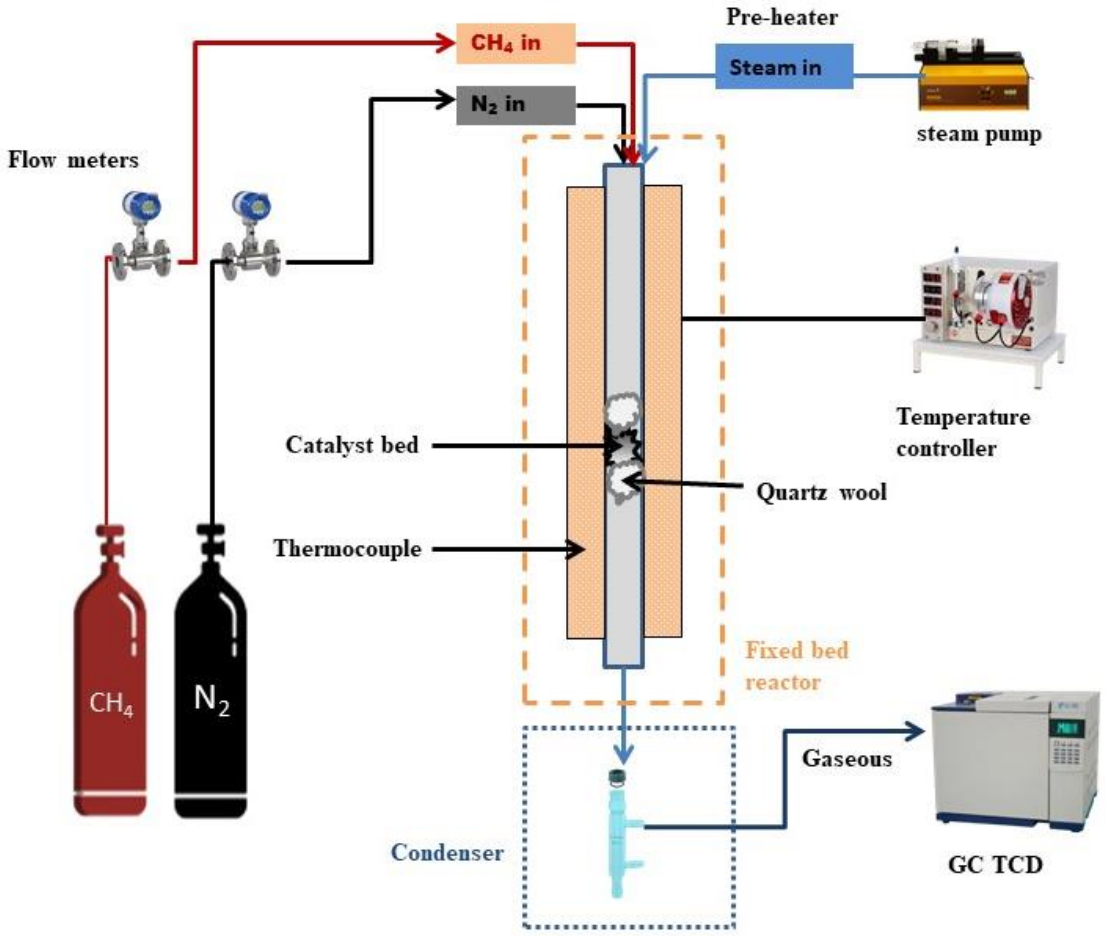

Fig 3.2 The experimental setup for steam reforming of methane on a fixed bed reactor

References

1. Munawar, M.A., et al., *Biomass ash characterization, fusion analysis and its application in catalytic decomposition of methane.* Fuel, 2021. **285**: p. 119107.
2. Raza, J., et al., *Methane decomposition for hydrogen production over biomass fly ash-based CeO_2 nanowires promoted cobalt catalyst.* Journal of Environmental Chemical Engineering, 2021. **9**(5): p. 105816.
3. Ayesha, M., et al., *Sorption enhanced steam reforming of methane over waste-derived CaO promoted MgNiAl hydrotalcite catalyst for sustainable H2 production.* Journal of Environmental Chemical Engineering, 2022. **10**(3): p. 107651.
4. Abbas, S.Z., V. Dupont, and T. Mahmud, *Kinetics study and modelling of steam methane reforming process over a NiO/Al2O3 catalyst in an adiabatic packed bed reactor.* International journal of hydrogen Energy, 2017. **42**(5): p. 2889-2903.
5. Palmer, C., et al., *Dry reforming of methane catalysed by molten metal alloys.* Nature Catalysis, 2020. **3**(1): p. 83-89.
6. Hao, Z., et al., *Characterization of aerogel Ni/Al2O3 catalysts and investigation on their stability for CH4-CO2 reforming in a fluidized bed.* Fuel Processing Technology, 2009. **90**(1): p. 113-121.
7. Wu, H.-C., Z. Rui, and J.Y. Lin, *Hydrogen production with carbon dioxide capture by dual-phase ceramic-carbonate membrane reactor via steam reforming of methane.* Journal of Membrane Science, 2020. **598**: p. 117780.
8. Meloni, E., et al., *Ultracompact methane steam reforming reactor based on microwaves susceptible structured catalysts for distributed hydrogen production.* International Journal of Hydrogen Energy, 2021. **46**(26): p. 13729-13747.
9. Palma, V., et al., *Catalysts for methane steam reforming reaction: evaluation of CeO2 addition to alumina-based washcoat slurry formulation.* C, 2020. **6**(3): p. 52.

Chapter 4

Results and discussions

4.1 Physicochemical properties of a catalyst

The synthesized catalysts and catalyst support (AC) structures were investigated using XRD analysis, which is shown in Fig 4.1. The best reported catalytic activity, according to the study, is found in AC and 5%Co@AC. The diffraction patterns validate the existence of the active metal and carbon as shown by the appropriate JCPDS values in Table 4.1. According to the diffraction patterns, all of the material devoted to distinctive carbon has a peak visible at an angle (2θ) of 29.31° (110). Graphitic carbon is said to have contributed to the peak at 26.04° (220) [1] which becomes prominent in all catalysts as a result of the metal-graphitic combination [2, 3]. Additionally, the broad peak that can be seen from 23.10° to 43.29° is one of the distinctive peaks of carbon materials. The axis of the graphite structure is also thought to be responsible for the faint and wide C (100) peak at 2θ = 40°–50° [4]. Similar to this, tiny peaks are seen at a 2θ ° angle: (using JCPDS # 72-2091) Carbon peaks may be found at 29.49°, 42.19°, 52.31°, 61.19°, 69.27°, and 77.13° with planes (110), (200), (211), (220), (013), and (222), respectively. This is a characteristic peak of carbon materials. The large peak broad peak at 2θ 23.4° to 40° corresponds to the amorphous carbon structure. The weak and broad C(100) peak at 2θ = 40°-50° is attributed to the axis of the graphite structure [4].

The peak formation of the carbon materials was found to be wide, and the width indicates the amorphous nature of the produced particles [5-7]. Although there are no prominent peaks observed in XRD results. The reason may be the active metal samples are properly dispersed over the catalyst support surface. Sometimes the XRD instruments are not very sensitive to a small number of active metals[8, 9]. However, small peaks are observed at 2θ angle: (with JCPDS # 72-2091) 29.49°, 42.193°, 52.315°, 61.199°, 69.278°, and 77.136° having planes (110), (200), (211), (220), (013) and (222) respectively corresponds to carbon peaks. The peaks at 26.8°, 44.1°, 56.0°, and 65.4° are attributed to the presence of the Co metallic phase on the adsorbent surface [10].

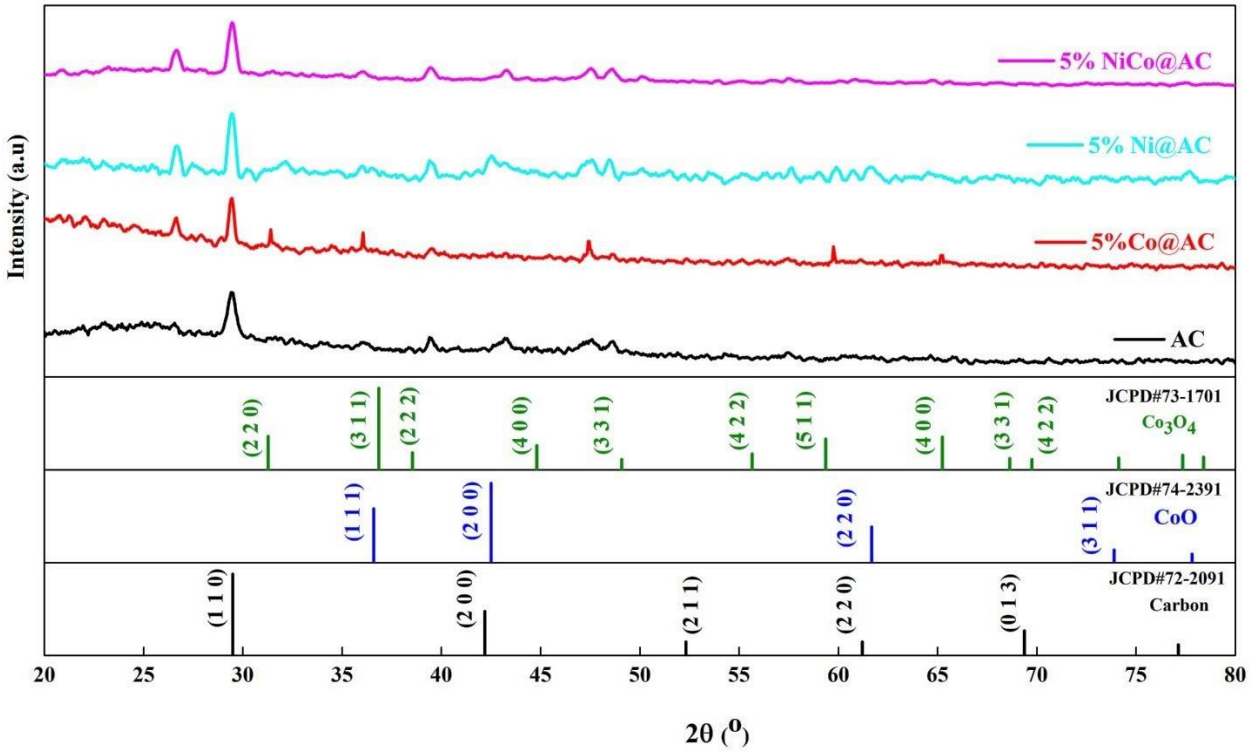

Fig 4.1 The XRD analysis of AC, 5%Co@AC, 5%Ni@AC, and 5%NiCo@AC catalysts

.Table 4.1 XRD analysis of the 5%Co@AC catalyst

	2 θ (degree)	**hkl indices**	**JCPDs #**
Carbon	29.490	(1 1 0)	JCPD#72-2091
	42.193	(2 0 0)	
	52.315	(2 1 1)	
	61.199	(2 2 0)	
	69.278	(0 1 3)	
	77.136	(2 2 2)	
CoO	36.591	(1 1 1)	JCPD#74-2391
	42.506	(2 0 0)	
	61.679	(2 2 0)	

	73.899	(3 1 1)	
	77.782	(2 2 2)	
Co_3O_4	31.272	(2 2 0)	JCPD#17-1701
	36.874	(3 1 1)	
	38.549	(2 2 2)	
	44.811	(4 0 0)	
	49.084	(3 3 1)	
	55.657	(4 2 2)	
	59.358	(5 1 1)	
	65.237	(4 0 0)	
	68.631	(3 3 1)	
	69.744	(4 2 2)	
	74.123	(6 2 0)	

It is evident from the XRD pattern of the Co nanoparticles that the diffraction peaks at scattering angles (2θ) of 44.31° and 51.65° are assigned to scattering from the (111) and (200) planes of the Cobalt crystal lattice. This would indicate that nanoparticles having the same crystal structure as bulk Co have been formed. When the percentage of O_2 is increased to 2.3%, we begin to observe the formation of cobalt oxide (CoO) together with trace amounts of cobalt as confirmed by XRD [11]. The existence of peak indexing at (111), (200), (220), and (311) (with JCPDS#74-2391) is dedicated to the CoO phase. There are also diffraction patterns recorded corresponding to Co_3O_4 at 36.591 (111) and two planes (400) at 44.811^o and 65.237^o (JCPDS# 73-1701) [12]. The characteristic reflection peak at 36.8°, associated with Co3O4, was observed for the calcined catalysts [13]. The presence of Co in the metallic form was confirmed by XRD patterns, indicating that during pyrolysis Co ions were reduced to Co crystallites with zero oxidation state, which stimulated the graphitization of gaseous carbon from the broken down organic ligands and another carbon source [14]. The crystallite size is 35.304 nm calculated by using Scherrer equation Eq. (44). The result is the same as reported by literature [15]. The catalyst with a small

crystallite size appears to be effective throughout the volume and has a greater advantage in catalytic activity [16].

$$D = \frac{k\lambda}{\beta \cos\theta} \tag{44}$$

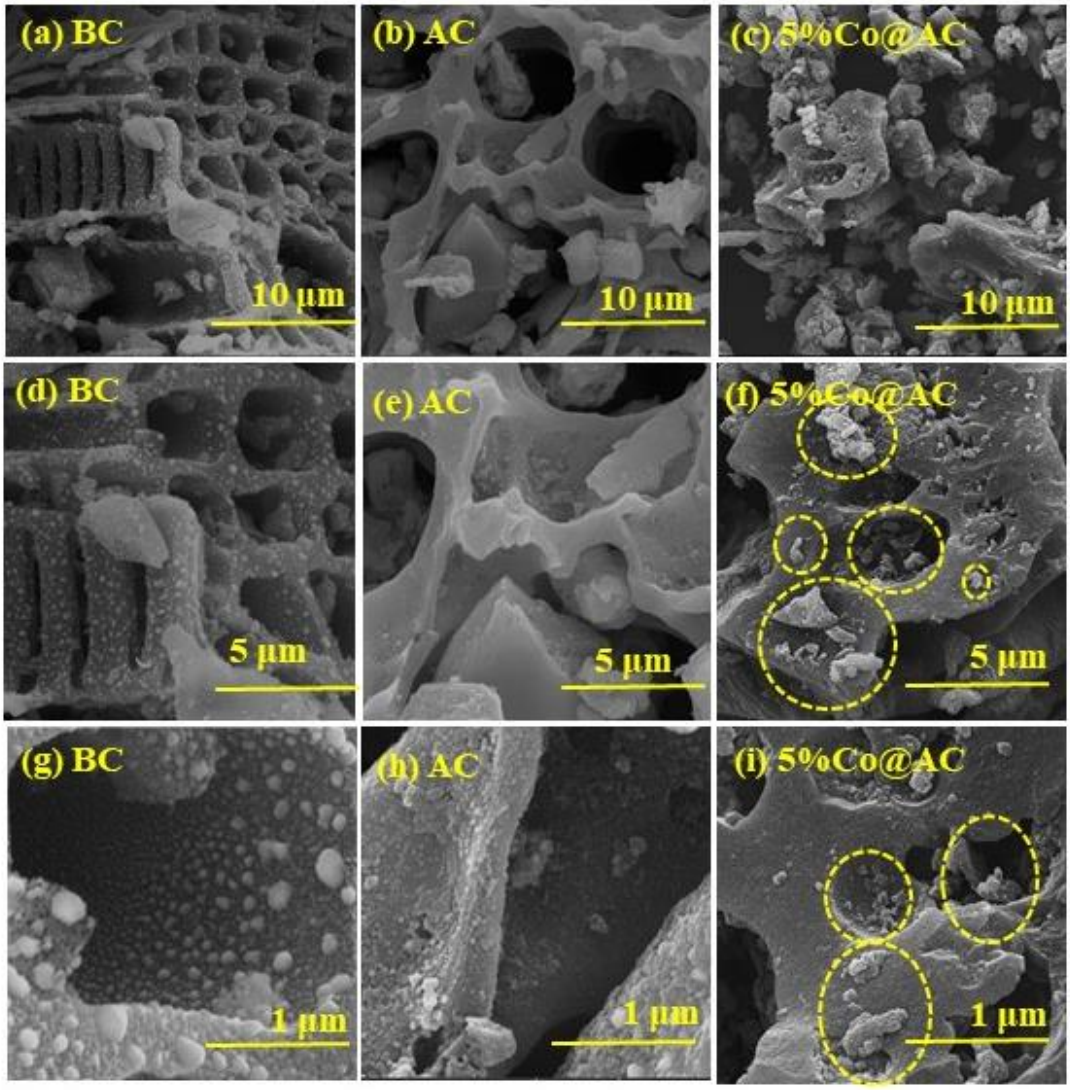

Fig 4.2 SEM analysis images of (a, d, g) BC, (b, e, h) AC, and (c, f, i) 5%Co@AC

Scanning electron microscopy (SEM) is employed for the surface morphology. Fig. 4.2 illustrates the images of untreated carbon (BC), AC catalyst support, and 5wt.% Cobalt-loaded

activated carbon (5%Co@AC) at different magnifications. The images show the clear round pores high in AC catalyst support which essentially provides a high surface area for better loading of Cobalt particles [17].

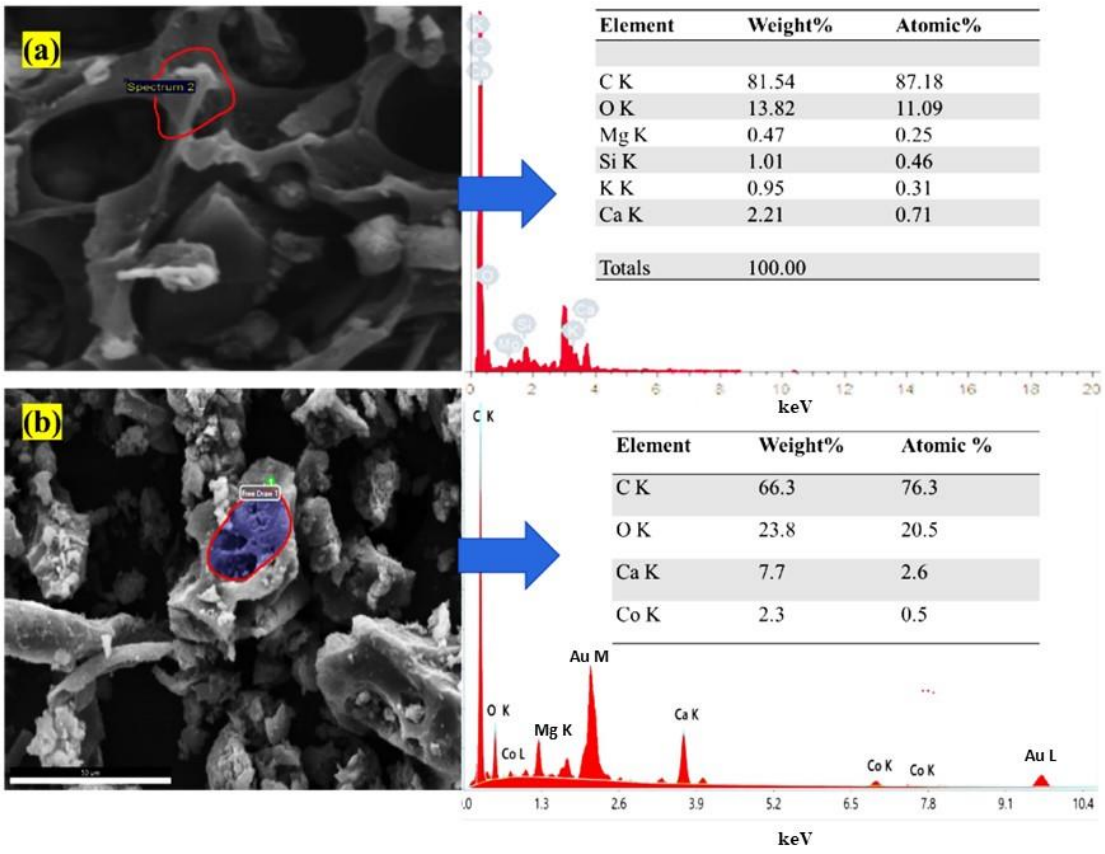

Fig 4.3 EDX analysis of (a) AC and (b) 5%Co@AC

Literature suggests that H_2O_2 modification of carbon improves the porosity and surface area by removing the inorganic compounds and impurities [18]. The diameter of round pores observed in the AC support catalyst ranges from 9-13 nm. Whereas the Cobalt can be seen scattered on the surface and internal cavities of the catalyst support and covered the pores of AC [19]. Thus, the well-developed porosity and surface area increased the cobalt particle distribution. In the case of 5%Co@AC, the AC can be seen in the low-density dark colour whereas the cobalt particles are visible high dense light white colour. There are no clusters or agglomeration has been observed. The partial blockage of pores not predominantly noted, which

is might be associated with the filling of active metal in the pores and the surface of catalyst support [20].

Fig. 4.3 represents the EDX of AC catalyst support and 5%Co@AC. There are various elements in both samples. AC has a greater percentage of carbon 81.54%, and the presence of oxygen is attributed to the formation of metallic oxides in the sample as discussed in XRD analysis, the oxygen percentage greater than 2.3% gives metallic oxides. Whereas 5%Co@AC retained the carbon percentage up to 66% while Co content was 2.3 wt. % as detected by EDX. The peaks detected in ranges of 1.2 keV to 2.2 keV correspond to gold coating.

To identify the functional groups and structural bonds present in the material, an FTIR analysis was conducted. Even though materials associated with AC mainly consist of carbon, they also contain minor amounts of heteroatoms such as oxygen, nitrogen, hydrogen, and sulfur. Therefore, it's crucial to look at the material's structural and chemical makeup [21]. Fig. 4.4 shows the infrared (IR) spectrum of hemp, AC, and 5%Co@AC, whereas Table 4.2 represents the correlation table.

Table 4.2 The correlation table of Fourier Transform Infrared spectroscopy

Wavenumber (cm^{-1})	**Vibration**	**Compound Class**
3301	O−H	alcohol
2926	C−H	alkane
1613	C=C	Conjugated alkene
1033	C−N	amine
1420	O−H	Carboxylic acid
881	C−H	1,2,4 trisubstituted
717		Benzene derivative

In the case of the IR spectrum of Hemp at top of the figure, as shown, the wave absorbed from 3000 cm-1 to 3600 cm-1, maxima at around 3290 cm-1 attributed to O-H stretching of hydroxyl group corresponds to adsorb water molecules[22, 23]. The peak at 1630 cm-1 is because of the protein amide I consequently the C=O stretching vibration, whereas, at 1530 cm-1 is due to amide II of C-N stretching alongside N-H bending [24]. The C-H stretching at 2929 cm-1

corresponds to methyl and methylene groups [22]. There is weak absorbance at around 1700 cm-1 represents the C=O, which corresponds to Carboxylic ester present in pectin and waxes [25]. The absorbance at 1020 cm-1 represents C-O stretching attributed to alcoholic groups[26]. The bands at 1420 cm−1 correspond to -CH2 stretching [23]. Another broadband in the 1470–1330 cm−1 region consists of a series of overlapping absorption bands which are ascribable to the deformation vibration of surface hydroxyl groups and in-plane vibrations of C−H in various C=C−H structures [27].

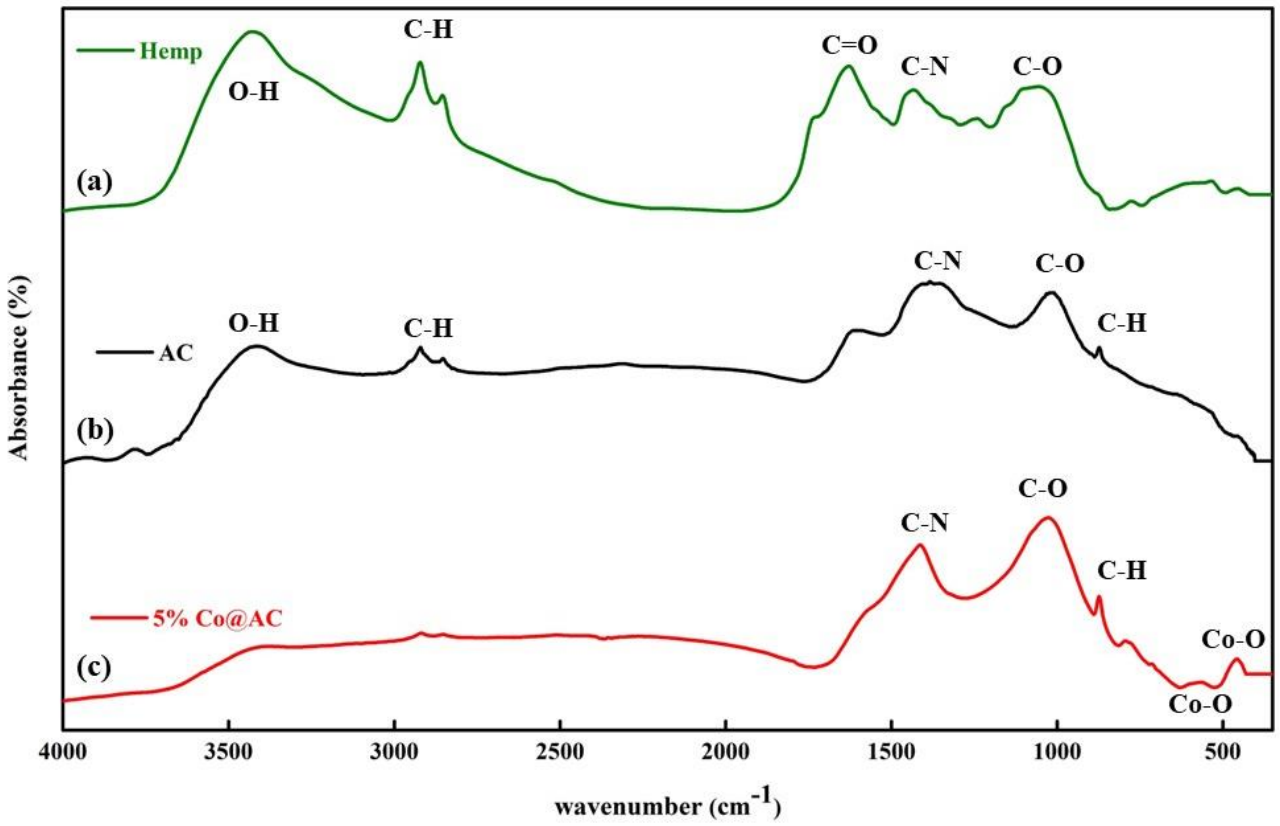

Fig 4.4 FTIR analysis of (a) Hemp (b) AC and (c) 5%Co@AC

A weak absorption sharp band at 880 cm−1, is usually attributed to the out-of-plane deformation mode of C−H, which represents a sudden decrease of monosubstituted C−H. An increase of isolated C−H in variously substituted benzene rings suggests a progressive substitution of C−H bonds in the aromatic system and the formation of new C−R bonds [27]. As Fig 4.4(b) illustrates that AC somehow retains most of the functional groups. Whereas, In the case of 5%Co@AC, O-

H and C-H groups are faded. As TGA studies also support the idea that up to 100° C the moisture and volatile matter start to release during the pyrolysis process. Furthermore, the O-H peak almost vanishes because of calcination. Moreover, the characteristic vibration at 450 cm-1 is the Co-O stretching of Cobalt oxide as shown in Figure 6 (c) [28]. There is small wide peak absorbed at 576 cm−1 is characteristic peak of Co-O that is stretching vibration because of Co3O4 [28, 29].

The surface area and pore characteristics of the material are calculated by N_2 adsorption-desorption BET analysis at 77.3 K bathing temperature. Before measurement, the samples were subjected to outgassing at a temperature of 300 °C for 10 h stay time in a vacuum to clean and dry the surface. The N_2 adsorption-desorption isotherm of AC and Cobalt catalyst (5%Co@AC) is given in Fig. 4.5. According to the International Union of Pure and Applied Chemistry's (IUPAC) classification, the isotherm of activated carbon (AC) displays type I isotherms, which denotes that the carbon is microporous. The platform for Type I isotherms often has a horizontal or nearly horizontal appearance, and the adsorption isotherm directly meets the line $P/P_o = 1$ in most cases. The quantities adsorbed sharply rise at the low relative pressure zone (P/P_o 0.2), as demonstrated in the initial stage. This indicates that the microporous structure is where most nitrogen molecules are adsorbed.[30]. The BET surface area calculated from the Density Functional Theory (DFT) cumulative surface area function of AC and 5%Co@AC is 46.39 m^2/g and 179.565 m^2/g respectively. The pore volume determined for AC and 5%Co@AC is 0.045 cm^3/g and 0.106 cm^3/g respectively. Whereas the pore radius of AC and 5%Co@AC is 0.615 nm and 1.814 nm respectively as given in Table 4.3.

Table 4.3 The surface area, Pore volume, and pore radius of AC and 5%Co@AC calculated by the DFT cumulative surface area function

Sample name	**S_{BET} (m^2/g)**	**Pore volume (cm^3/g)**	**Half pore width (nm)**
AC	46.39	0.045	0.615
5%Co@AC	179.3	0.106	1.814

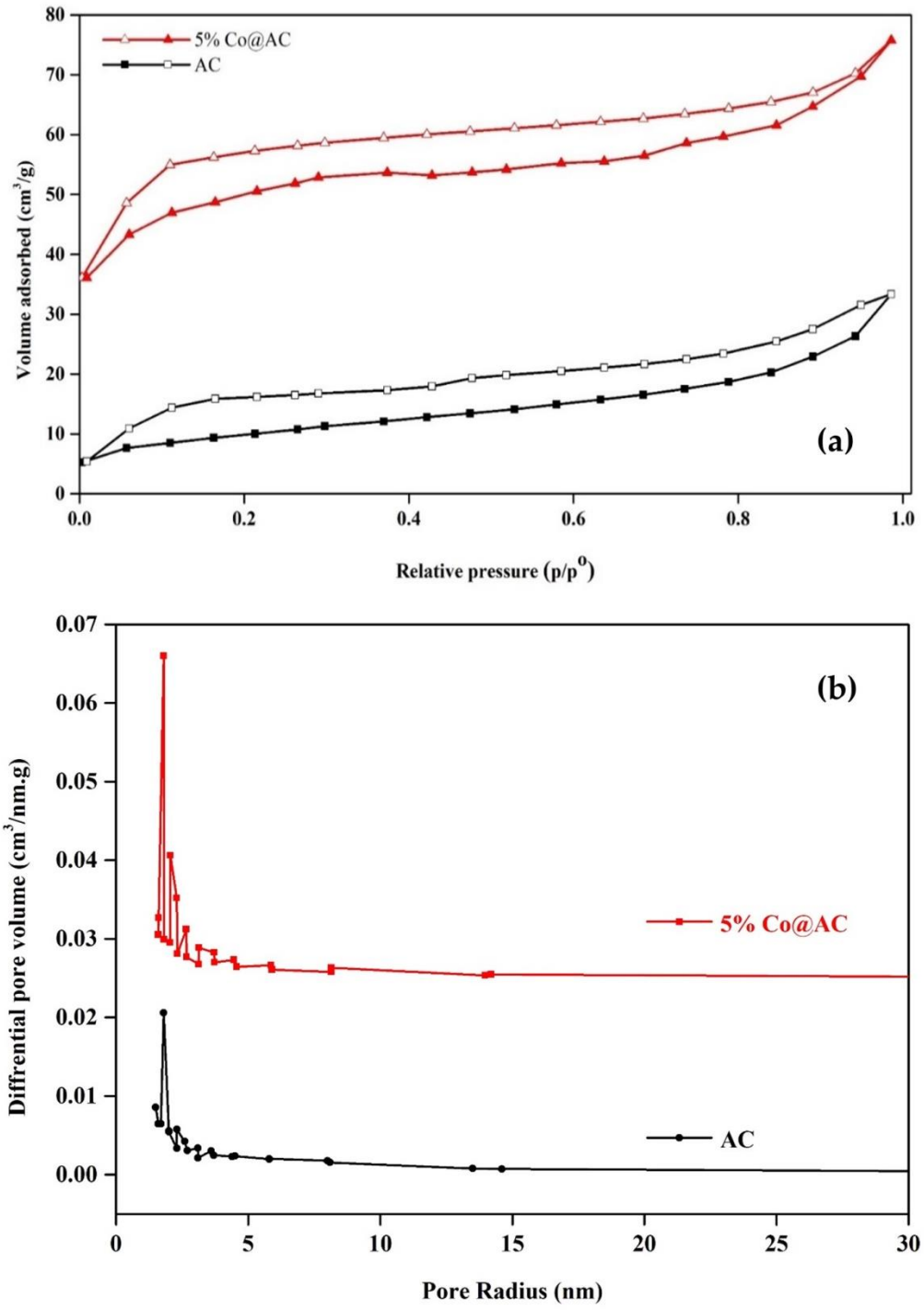

Fig 4.5 **(a)** N_2 adsorption (closed symbols)-desorption (open symbols) isotherm of AC and 5%Co@AC (b) Pore size distribution (BJH) of AC and 5%Co@AC

As it is evident that catalyst support has a smaller surface area, porosity, and pore size relatively catalyst composite. Generally, the BET surface area of material is inversely proportional to the pore size radius since composites give a smaller surface area than the support. This is a very rare event that is being observed sometimes that composite catalyst gives larger surface area than that of support. Amin et al [31] also reported a phenomenon where composite material gives more surface area than the catalyst support. One explanation of such a phenomenon is that porosity is also one of the parameters that define the surface area of the material. Sometimes in some cases, the material with small pore diameters shows lesser surface area because of the small number of pores per gram as seen in this case [32]. Another possibility is that the nature of metal and support also plays a crucial role in defining the surface area. The reason may be that the active metal sites oxidize the activated carbon creating more micropores thus increasing the surface area since XRD results reveal the presence of CoO and Co3O4 in the sample. Additionally, Fig 4.5 (b) shows the BJH model-calculated pore size distribution. The pore size distribution as it manifests spans from 1.5 nm to 14 nm in radius, with the bulk falling between 1.6 nm and 3.0 nm. According to the pore size distribution, the pore radius of 5%Co@AC is 1.80 nm, while that of AC is 1.59 nm.

The thermogravimetric analysis test is performed for thermal stability of catalyst support AC and Cobalt catalyst (5%Co@AC). The TGA analysis results are illustrated in Fig. 4.6(a-b). In both cases, the weight loss is distributed in four temperature ranges. Initially up to 100 °C, followed by roughly 650 °C and some weight loss observed after 700 °C. In the case of activated carbon-based materials, at the initial stages of temperature, the organic matter decomposes then obtained intermediates, and activating reagents decompose at elevated temperatures. At the beginning 100 °C, the moisture and volatile matters start to decompose resulting in weight loss. As temperature rises the organic matter typically lignin cellulose, and hemicellulose decomposes. Further heating results in weight loss because of the carbonization and tar formation of gaseous products and volatiles contributing to weight loss [33]. Some of the same kind of behaviour has been observed in this case. The weight loss of 4wt.% occurred at around 100 °C in both cases as temperature rises are attributed to desorption of physiosorbed moisture, decarbonization, and sometimes combustion of unreacted nitrates [34-36]. In addition, literature

[34] ascribes that further weight losses correspond to the release of carbon dioxide and carbon monoxides in carbon material cases.

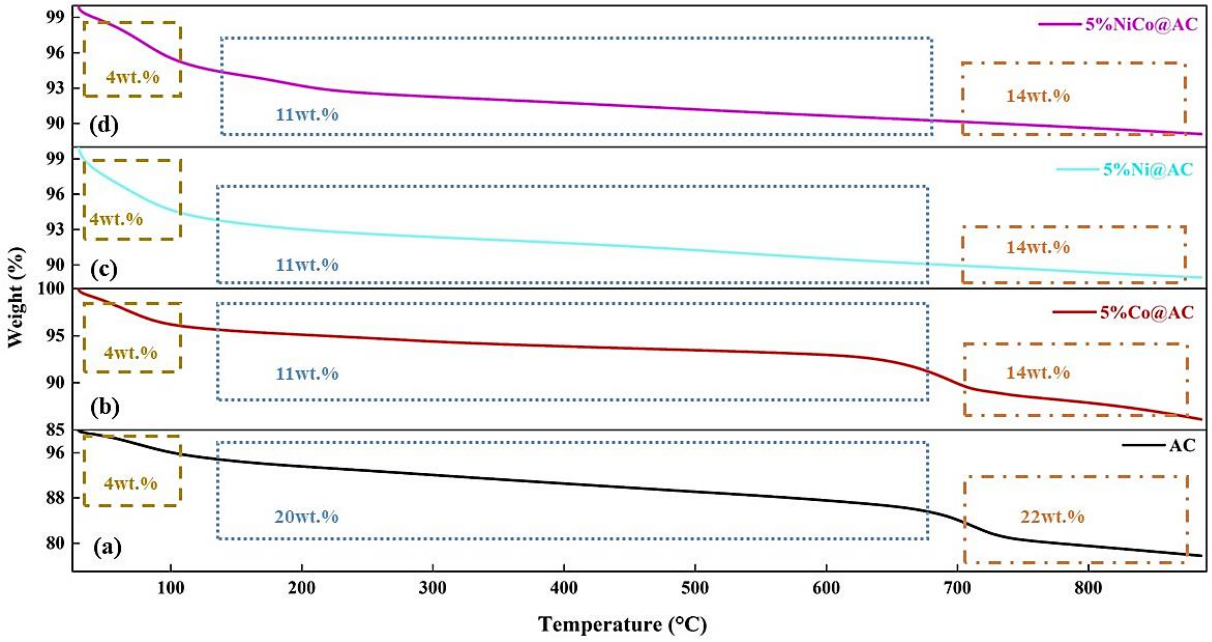

Fig 4.6 TGA analysis results of AC (a), 5%Co@AC (b), 5%Ni@AC(c) and 5%NiCo@AC(d)

4.2 Catalyst Performance analysis

4.2.1 Catalyst activity test

The SMR catalytic activity was carried out in a fixed bed reactor at a temperature of 750 °C for AC support, sequentially impregnated monometallic Cobalt (5%Co@AC), monometallic nickel (5%Ni@AC), and co-impregnated bimetallic Ni-Co (5%NiCo@AC) catalyst for 18 h testing time. Fig. 9 (a) shows the CH_4 conversion results of all synthesized material. As clear from the result, the CH_4 conversion for 5%Co@AC is best recorded that is 97.69% among all other catalysts. The high CH_4 conversion for 5%Co@AC is since the Cobalt shows good interaction between the support that is associated with reduced Co sites with metal loadings[35]. It can be seen from the results that the CH_4 conversion order becomes for all samples as follow: 5%Co@AC > 5%Ni-Co@AC > 5%Ni@AC > AC. There is no CO_2 gas has been detected through the activity indicating that no WGS reaction occurred.

Fig. 9 (b) represent the H_2 production and Fig. 9 (c) represents CO production. As it is clear in results H_2 production and CO production of 5%Co@AC are recorded as 66.08% and 10.39% respectively, and that is also the best record among all synthesized materials. Whereas the H_2 production for AC, 5%Ni@AC and 5%NiCo@AC becomes 53.36%, 61.02% and 65.89% respectively. Likewise, the CO production for AC, 5%Ni@AC and 5%NiCo@AC becomes 5.56%, 10.71% and 8.88% respectively. Delvin et al [37] reported that at low-temperature Ni catalyst gives better selectivity of hydrogen because it requires less activation energy than Co catalyst. On the other hand, Co catalyst is suggested highly effective at elevated temperature reactions for better hydrogen selectivity which is less prone to catalyst deactivation. Thus, Co catalysts have more leverage over Ni catalysts for high temperatures. This phenomenon is also understandable through thermodynamics following C-C bond cleavage and C-O bond cleavage. The high-temperature reactions occur at expense of the net consumption of water. It is worth mentioning that hydrogen selectivity of Co catalyst is high because the methane content in organic compounds is high over nickel catalyst since the C-C bond cleavage over nickel relative to the rate of C-O bond cleavage compared to cobalt catalysts.

From Fig 9 (d), the H_2/CO ratio of 5%Co@AC is calculated as 2.67, which is less than other materials. This is because Cobalt supported catalyst increases the reverse water gas shift reaction that produces more CO relatively other materials [19]. Although, enormous research held on Ni-Co bimetallic co-impregnation and monometallic Ni, Co sequential impregnation catalyst activity for many reforming techniques such as SR reaction of coal tar, toluene, and phenol. Many of them reported bimetallic Ni-Co as the best catalyst due to the fact of synergetic effect and better ability of high dispersion of active sites [38-40]. However, there are some exceptions to the principles. Grzegorz et al [41] suggest that catalyst support also plays a key role in defining the activity of the catalyst. Another reason is a larger metal crystallite favours the carbon deposition that deteriorates the long-term catalyst performance and becomes the reason for catalyst deactivation hampering the catalyst stability. Whereas the catalysts with smaller metal crystallites do not deposit the carbon too much that disturbs the catalytic activity thus giving more stability and fewer chances of catalyst deactivation in the process. The high dispersion of metal over the catalyst support is also describes the better activity of catalyst. As it

is clear from the XRD and SEM results of Cobalt catalyst that high dispersion is observed in this case.

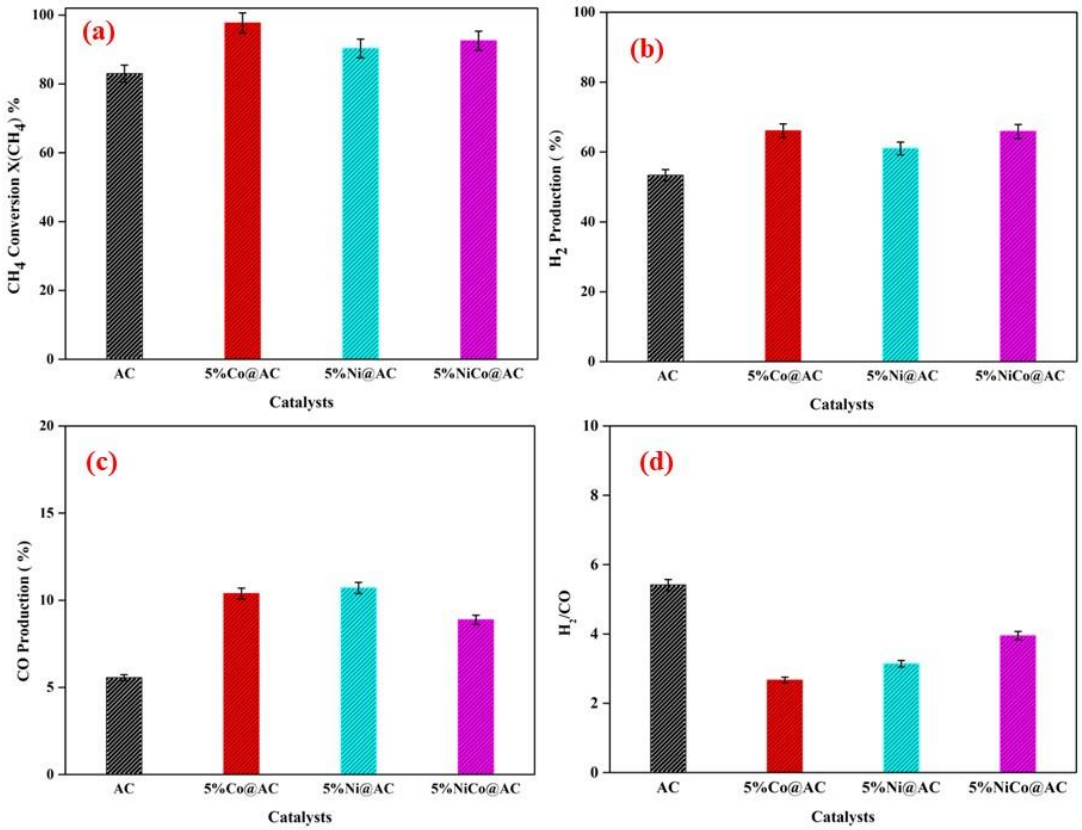

Fig 4.7 The catalytic activity of synthesized catalyst at 750 °C, H_2O/CH_4=2, in terms of (a) methane conversion XCH_4(%), (b) hydrogen production H_2(%), (c) carbon monoxide production CO(%), and (d) H_2/CO

Fig. 10 (a,) exhibits the line-graph representation of methane conversion, Fig. 10 (b) shows hydrogen production, Fig. 10 (c) represents the carbon monoxide production and Fig 10(d) shows the H_2/CO ratio with each sample along the time of sampling. As it is also evident from bar graph results that until 6-7 samples the methane conversion was almost the same for all the samples. After 7 samples the conversion of Ni and bimetallic catalyst started decreasing whereas, the Co catalyst shows somehow linear behaviour. In the hydrogen production graph, there was no dramatic difference among all samples has been observed as it is also clear from the hydrogen

production graph that roughly one point difference among them i-e 5%Co@AC > 5%NiCo@AC > 5%.Ni@AC>AC gives 66.08% > 65.89% > 61.02%>53.36% respectively.

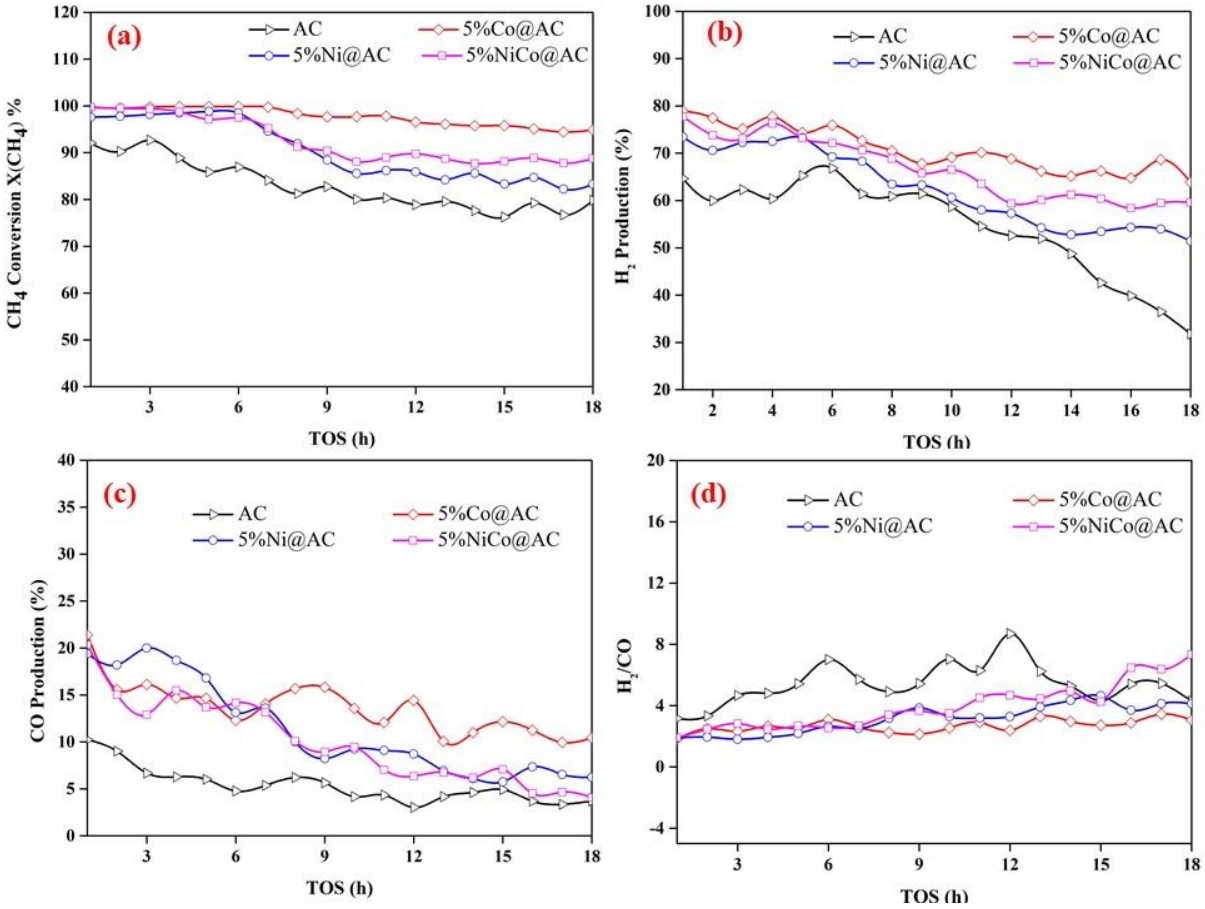

Fig 4.8. The graphical representation of (a) methane conversion XCH_4(%), (b) hydrogen(H_2) production, (c) carbon monoxide (CO) production, and (d) the ratio of H_2/CO. 2.2 Stability analysis

4.2.2 Stability analysis

From the catalytic activity of all catalysts, the cobalt impregnated catalyst (5%Co@AC) is deduced as the best-performed catalyst among other catalyst samples. The stability test of the 5%Co@AC catalyst is determined by running the catalyst for TOS 44 h at 750 °C, GHSV=6000 ml/h.gcat as presented in Fig. 11. As clear from the presented figure the methane conversion is

gradually decreasing over time. The methane conversion is consistent with previous catalytic test, starts from 99.70% and gradually decreases to 87% where it becomes stabilized since the Cobalt shows good interaction between the support that is associated with reduced Co sites with metal loadings[35].

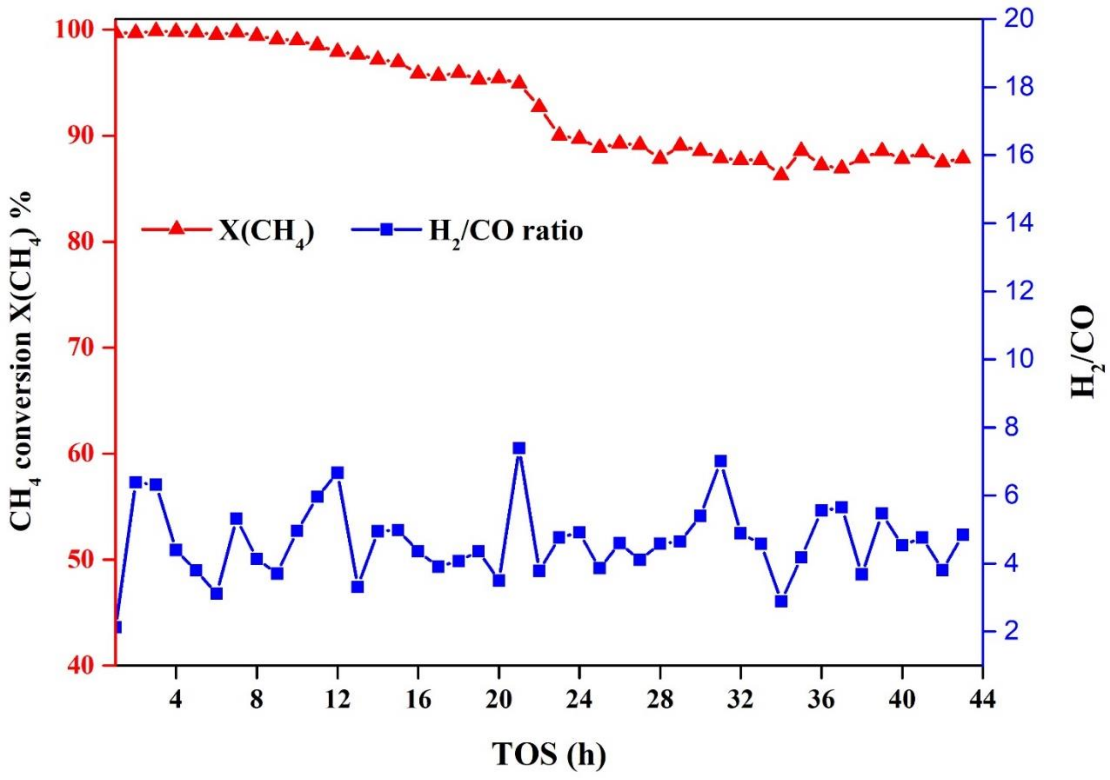

Fig 4.9 The catalytic stability test of 5%Co@AC for SMR reaction. Experimental conditions: at 750 °C, H_2/CH_4=2, TOS=18h, GHSV=6000 ml/h.gcat

The average methane conversion in total screening time TOS 44 h becomes 93.17%. It also shown that there is a little dip observed in methane conversion at 18 h indicates the deficiency of necessary oxygen to convert methane [42]. The catalytic performance is also governed by particle morphology, shape of catalyst support and the doping in lower valence cation. It is also shown that the catalytic behaviour relies upon the catalyst preparation process and the characteristics of catalyst support significantly influences the surface acidity like redox reaction

of Co species [43]. Whereas the H_2/CO ratio varies between 2-7 and the average value happens to be around 4.5. Furthermore, there is no more decrease in the conversion of methane indicating more resistance towards catalyst deactivation. The higher H_2/CO ratio also depends upon S/C inlet. Anyhow the high H_2/CO ratio avoids the catalyst deactivation and is highly recommended [44].

4.3 Characterization of spent catalyst

Fig. 4.10 represents the XRD analysis of the spent 5%Co@AC catalyst that has been checked for stability analysis for 18 h. The broad peak at 2θ (hkl)= 23.5° (002) and peak at 43.8° (101) correspond to graphite carbon in the sample [45, 46]. Although there are no distinct peaks observed. However, some weak peaks are detected at angles 2θ: 26.05°, 44.317°, 51.38°, and 62.43°. According to the literature [47], the peak at 26.05° corresponds to Cobalt oxide crystallites (Co_2O_3).

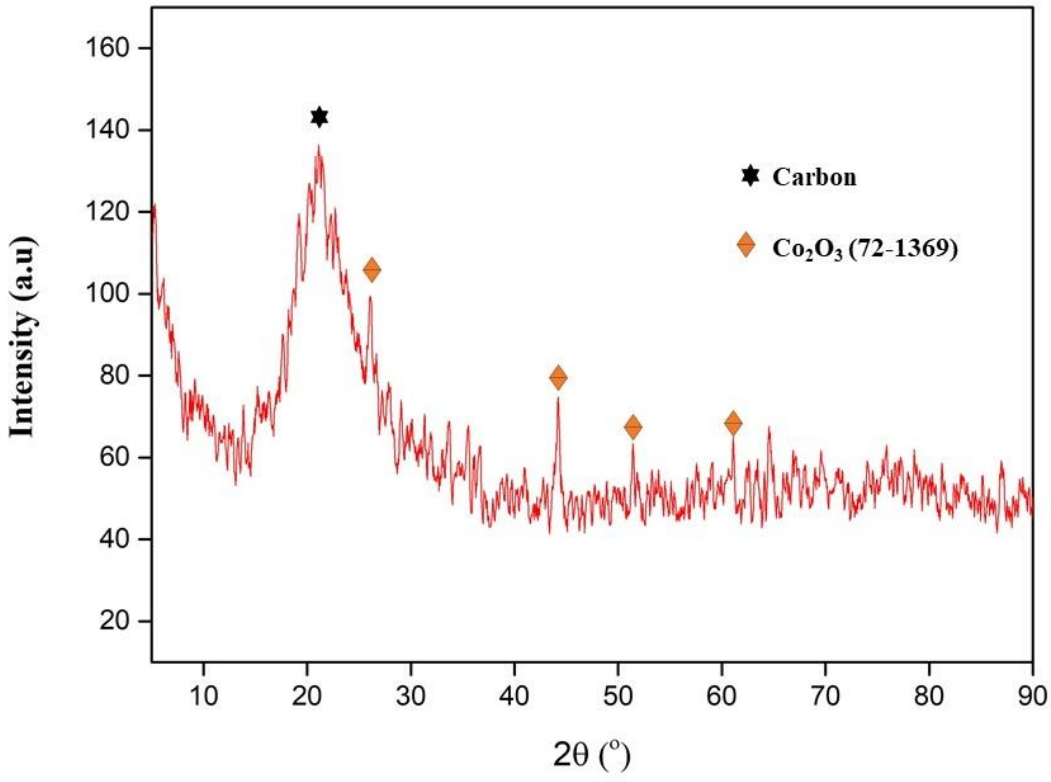

Fig 4.10 XRD analysis of spent catalyst 5%Co@AC after 44h TOS

The SEM micrograph images of spent 5%Co@AC are represented in Fig. 4.11(a-b). As the SEM micrographs demonstrate that there is a significant textural change occurred in the spent catalyst. The surface of the spent catalyst is much smoother and contains small grains than a fresh catalyst. The rough surface of a fresh catalyst than spent is in agreement with the high surface area and porous structure which is a decrease in the spent catalyst as evident by BET analysis results which suggest the formation and deposition of carbon on the surface, that is because of the faster methane cracking rate than that of carbon removal by gasification reactions[48].

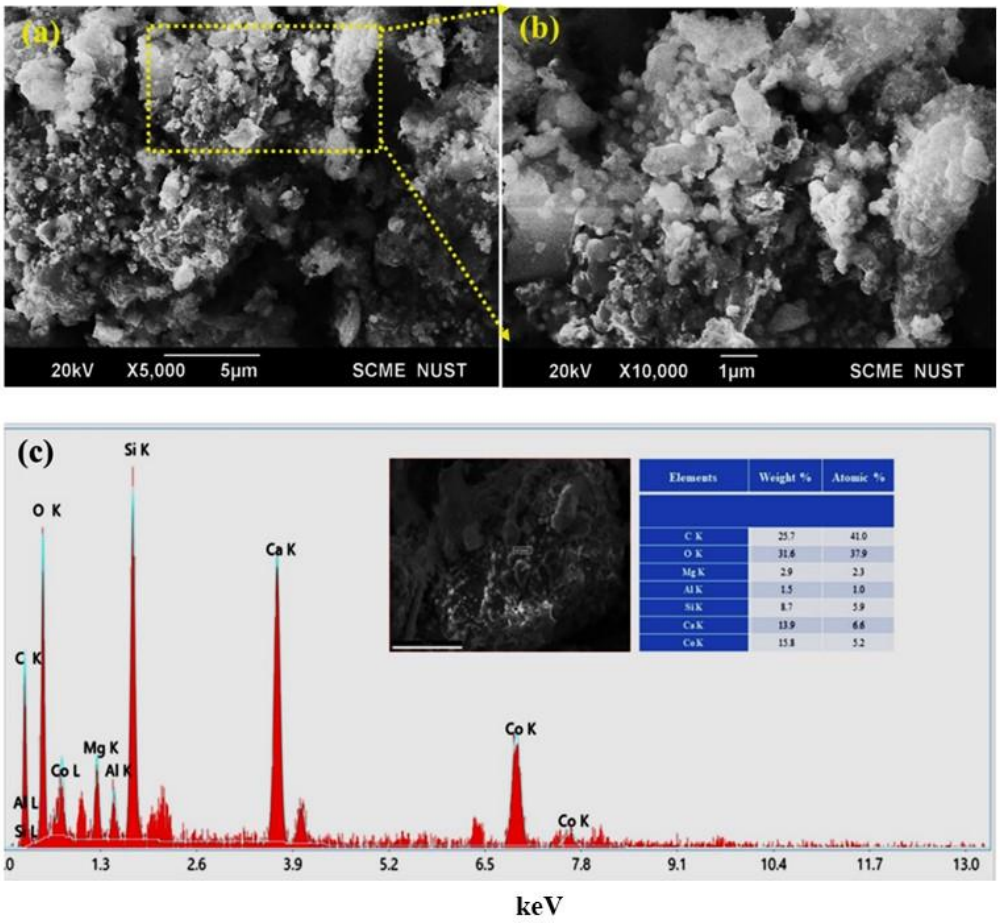

Fig 4.11 The SEM analysis of spent 5%Co@AC catalyst after 44 h TOS (a) 5µm and (b) 1µm (c) EDX analysis of spent 5%Co@AC catalyst after 44h TOS

Fig. 4.11(c) illustrates the elemental analysis EDX of 5%Co@AC spent catalyst. The carbon and Cobalt have been significantly detected along with some other elements as evident from XRD results also. Some carbonaceous species were also formed due to the reactive phase during the reaction, a carbon gasification at high temperature was expected and produced CO that had a higher syngas ratio[35].

Fig. 4.12(a) shows the N_2 physisorption isotherm of the spent Cobalt catalyst (5%Co@AC) from the stability test analysis. The figure exhibits the combination of type I and IV isotherm which proves the presence of micropores mad mesopores in the sample [49]. Table 4.4 represents the surface area, pore-volume, and pore radius calculated by the DFT method of Cobalt spent catalyst. As it is evident from the BET results of fresh catalyst and spent catalyst that the surface area and pore volume are significantly decreased in the spent catalyst which suggests that pores are almost filled suggesting the deactivation of the catalyst.

Table 4.4 The surface area, Pore volume, and pore radius of spent 5%Co@AC were calculated by the DFT cumulative surface area function after 44 h TOS

Sample	**S_{BET} (m^2/g)**	**Pore volume (cm^3/g)**	**Half pore width (nm)**
Spent 5%Co@AC	14.25	0.007	0.615

Fig. 4.12(b) illustrates the TGA analysis result of the stability test spent 5%Co@AC. The TGA analysis is essential to determine the coke deposition on the spent catalyst. As the profile of TGA depicts, there is a no significant weight loss has been observed. Roughly 1% mass loss linearly with temperature was observed during the investigation. The mass loss regarded as the change of Cobalt oxide into metallic cobalt with the loss of oxygen [50]. This indicates the small carbon deposition on 5%Co@AC and catalyst shows greater stability as also cleared from SEM results

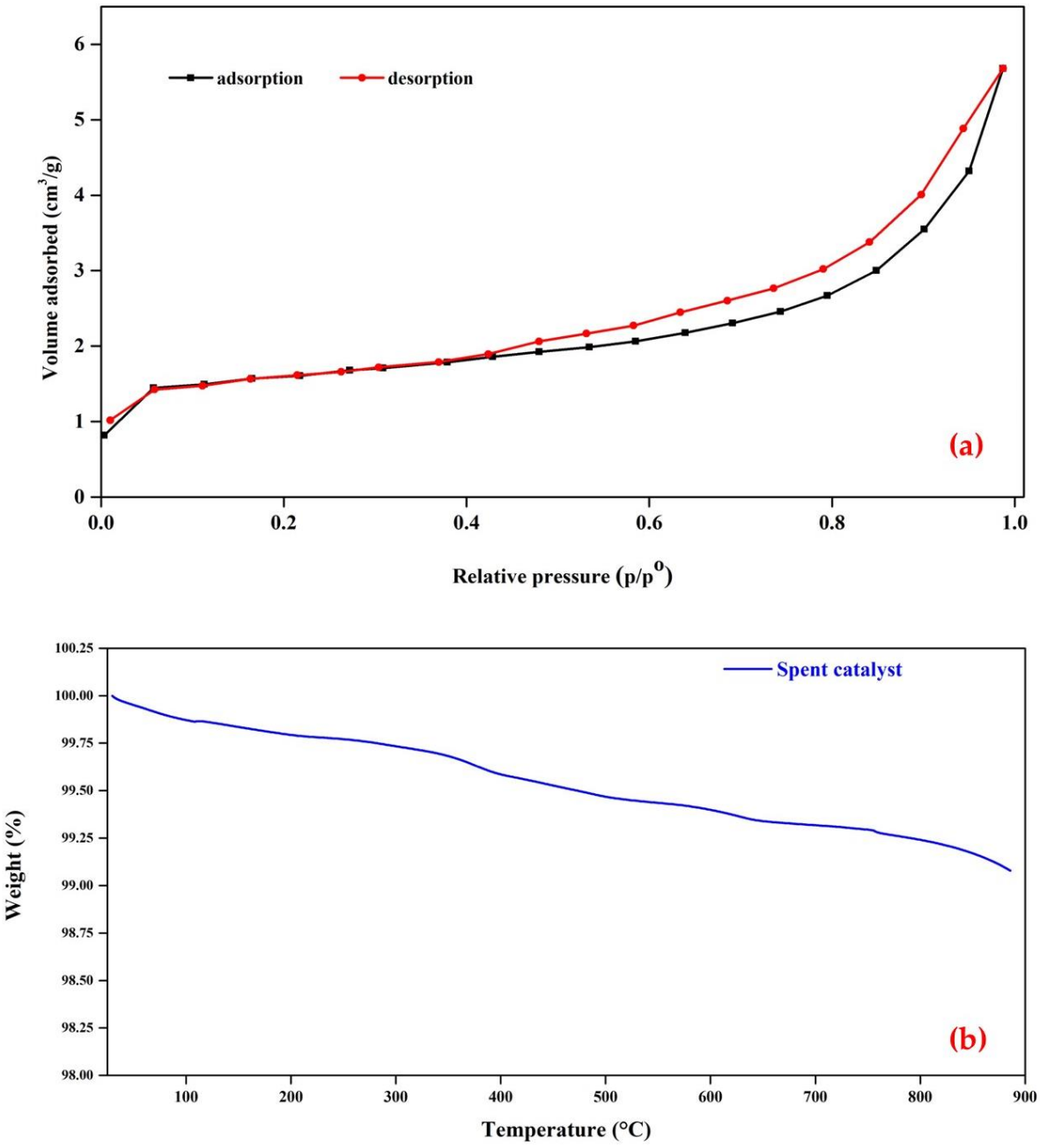

Fig 4.12 (a) BET analysis of spent catalyst 5%Co@AC after 44 h TOS. (b) TGA analysis of spent catalyst 5%Co@AC after 44 h TOS.

References

1. Fu, R., et al., *Formation of graphitic structures in cobalt-and nickel-doped carbon aerogels.* Langmuir, 2005. **21**(7): p. 2647-2651.

2. Zhong, Z., et al., *Nanosized nickel (or cobalt)/graphite composites for hydrogen storage.* The Journal of Physical Chemistry B, 2002. **106**(37): p. 9507-9513.

3. Takanabe, K., et al., *Titania-supported cobalt and nickel bimetallic catalysts for carbon dioxide reforming of methane.* Journal of Catalysis, 2005. **232**(2): p. 268-275.

4. Hossain, M.Z., et al., *High-surface-area mesoporous activated carbon from hemp bast fiber using hydrothermal processing.* C, 2018. **4**(3): p. 38.

5. Rajagopal, R.R., et al., *Activated carbon derived from non-metallic printed circuit board waste for supercapacitor application.* Electrochimica Acta, 2016. **211**: p. 488-498.

6. Mu, J., et al., *High photocatalytic activity of ZnO− carbon nanofiber heteroarchitectures.* ACS applied materials & interfaces, 2011. **3**(2): p. 590-596.

7. Islam, M.M., et al., *Heterogeneous route for the one-pot synthesis of N-arylamides from aldoximes and aryl halides using the CuO/carbon material.* ACS omega, 2017. **2**(12): p. 8600-8609.

8. Singhania, A. and A.N. Bhaskarwar, *Performance of Activated-Carbon-Supported Ni, Co, and Ni–Co Catalysts for Hydrogen Iodide Decomposition in a Thermochemical Water-Splitting Sulfur–Iodine Cycle.* Energy Technology, 2018. **6**(6): p. 1104-1111.

9. Sun, Y., et al., *Effect of different activated carbon support on CH4CO2 reforming over Co-based catalysts.* International Journal of Hydrogen Energy, 2018. **43**(3): p. 1497-1507.

10. Yahya, M.D., et al., *Characterization of cobalt ferrite-supported activated carbon for removal of chromium and lead ions from tannery wastewater via adsorption equilibrium.* Water Science and Engineering, 2020. **13**(3): p. 202-213.

11. Glaspell, G.P., P.W. Jagodzinski, and A. Manivannan, *Formation of cobalt nitrate hydrate, cobalt oxide, and cobalt nanoparticles using laser vaporization controlled condensation.* The Journal of Physical Chemistry B, 2004. **108**(28): p. 9604-9607.

12. Yahya, H.S.M., T. Abbas, and N.A.S. Amin, *Optimization of hydrogen production via toluene steam reforming over Ni–Co supported modified-activated carbon using ANN coupled GA and RSM.* International Journal of Hydrogen Energy, 2021. **46**(48): p. 24632-24651.

13. Mehrbod, M., et al., *Fischer-Tropsch synthesis: Direct cobalt nitrate reduction of promoted Co/TiO2 catalysts.* Fuel, 2019. **245**: p. 488-504.

14. Alotaibi, N., et al., *Cobalt–carbon/silica nanocomposites prepared by pyrolysis of a cobalt 2, 2'-bipyridine terephthalate complex for remediation of cationic dyes.* RSC Advances, 2020. **10**(30): p. 17660-17672.

15. Nethravathi, C., et al., *Ferrimagnetic nanogranular Co3O4 through solvothermal decomposition of colloidally dispersed monolayers of α-cobalt hydroxide.* The Journal of Physical Chemistry B, 2005. **109**(23): p. 11468-11472.

16. Ayesha, M., et al., *Sorption enhanced steam reforming of methane over waste-derived CaO promoted MgNiAl hydrotalcite catalyst for sustainable H2 production.* Journal of Environmental Chemical Engineering, 2022. **10**(3): p. 107651.

17. Izhab, I., M. Asmadi, and N.A.S. Amin, *Methane dry reforming using oil palm shell activated carbon supported cobalt catalyst: Multi-response optimization.* International Journal of Hydrogen Energy, 2021. **46**(48): p. 24754-24767.

18. Shen, B., et al., *Enhancing the absorption of elemental mercury using hydrogen peroxide modified bamboo carbons.* Fuel, 2019. **235**: p. 878-885.

19. Izhab, I., N.A.S. Amin, and M. Asmadi, *Dry reforming of methane over oil palm shell activated carbon and ZSM-5 supported cobalt catalysts.* International Journal of Green Energy, 2017. **14**(10): p. 831-838.

20. Yadav, B.R. and A. Garg, *Catalytic oxidation of pulping effluent by activated carbon-supported heterogeneous catalysts.* Environmental technology, 2016. **37**(8): p. 1018-1025.

21. Yakout, S. and G.S. El-Deen, *Characterization of activated carbon prepared by phosphoric acid activation of olive stones.* Arabian journal of chemistry, 2016. **9**: p. S1155-S1162.

22. Zhang, J., et al., *Characterization, preparation, and reaction mechanism of hemp stem based activated carbon.* Results in physics, 2017. **7**: p. 1628-1633.

23. Wang, Y., et al., *Hydrothermal preparation of highly porous carbon spheres from hemp (Cannabis sativa L.) stem hemicellulose for use in energy-related applications.* Industrial Crops and Products, 2015. **65**: p. 216-226.

24. Siano, F., et al., *Comparative study of chemical, biochemical characteristic and ATR-FTIR analysis of seeds, oil and flour of the edible fedora cultivar hemp (Cannabis sativa L.).* Molecules, 2019. **24**(1): p. 83.

25. Dai, D. and M. Fan, *Characteristic and performance of elementary hemp fibre.* Materials Sciences and Applications, 2010. **1**(06): p. 336.

26. Hossain, M.Z., et al., *High-surface-area mesoporous activated carbon from hemp bast fiber using hydrothermal processing.* C—Journal of Carbon Research, 2018. **4**(3): p. 38.

27. Yang, R., et al., *Preparation and N2, CO2 and H2 adsorption of super activated carbon derived from biomass source hemp (Cannabis sativa L.) stem.* Microporous and Mesoporous Materials, 2012. **158**: p. 108-116.

28. Zhang, F., et al., *Facile growth of mesoporous Co3O4 nanowire arrays on Ni foam for high performance electrochemical capacitors.* Journal of Power Sources, 2012. **203**: p. 250-256.

29. Hafeez, M., et al., *Green synthesis of cobalt oxide nanoparticles for potential biological applications.* Materials Research Express, 2020. **7**(2): p. 025019.

30. Hidayu, A., et al., *Characterization of activated carbon prepared from oil palm empty fruit bunch using BET and FT-IR techniques.* Procedia Engineering, 2013. **68**: p. 379-384.

31. Amin, M.H., J. Tardio, and S.K. Bhargava, *An investigation on the role of lanthanide promoters in promoted gamma-alumina-supported nickel catalysts for dry reforming of methane.* Chemeca Challenging Tomorrow, 2013.

32. Din, I.U., *Why the BET surface area of a catalyst (Metal/supp) higher than the support?* (2020).

33. Iwanow, M., et al., *Activated carbon as catalyst support: precursors, preparation, modification and characterization.* Beilstein Journal of Organic Chemistry, 2020. **16**(1): p. 1188-1202.

34. Contescu, C.I., et al., *Activated carbons derived from high-temperature pyrolysis of lignocellulosic biomass.* C, 2018. **4**(3): p. 51.

35. Mazhar, A., et al., *Performance Analysis of TiO_2-Modified Co/$MgAl_2O_4$ Catalyst for Dry Reforming of Methane in a Fixed Bed Reactor for Syngas (H_2, CO) Production.* Energies, 2021. **14**(11): p. 3347.

36. Hasnain, M.A.U., et al., *Partial oxidation of methane over CeO2 loaded hydrotalcite (MgNiAl) catalyst for the production of hydrogen rich syngas (H2, CO).* International Journal of Hydrogen Energy, 2021. **46**(74): p. 36663-36677.

37. Aman, D., et al., *Comparing nickel and cobalt perovskites for steam reforming of glycerol.* Molecular Catalysis, 2018. **452**: p. 60-67.

38. Yahya, H.S.M. and N.A.S. Amin, *Catalytic steam reforming of toluene for hydrogen production over nickel-cobalt supported activated carbon.* International Journal of Integrated Engineering, 2019. **11**(7): p. 209-218.

39. Tian, B., et al., *Monolithic biochar-supported cobalt-based catalysts with high-activity and superior-stability for biomass tar reforming.* Energy, 2021: p. 122970.

40. Wang, L., et al., *Catalytic performance and characterization of Ni–Co catalysts for the steam reforming of biomass tar to synthesis gas.* Fuel, 2013. **112**: p. 654-661.

41. Słowik, G., et al., *Influence of composition and morphology of the active phase on the catalytic properties of cobalt-nickel catalysts in the steam reforming of ethanol.* Materials Chemistry and Physics, 2021. **258**: p. 123970.

42. Wang, M., et al., *Reaction pathways of methane abatement in Pd-Rh three-way catalyst in heavy duty applications: A combined approach based on exhaust analysis, model gas reactor and DRIFTS measurements.* Chemical Engineering Journal, 2021. **422**: p. 129932.

43. Sohn, H. and U.S. Ozkan, *Cobalt-based catalysts for ethanol steam reforming: an overview.* Energy & Fuels, 2016. **30**(7): p. 5309-5322.

44. Chibane, L. and B. Djellouli, *Methane steam reforming reaction behaviour in a packed bed membrane reactor.* International Journal of Chemical Engineering and Applications, 2011. **2**(3): p. 147.

45. Zhang, J., et al., *Investigation of the supercapacitance of ruthenium-based/hemp stem activated carbon.* Journal of Physics and Chemistry of Solids, 2021. **153**: p. 110019.

46. Sreńscek-Nazzal, J., et al., *Activated Carbon Modification towards Efficient Catalyst for High Value-Added Products Synthesis from Alpha-Pinene.* Materials, 2021. **14**(24): p. 7811.

47. Shukla, P.R., et al., *Activated carbon supported cobalt catalysts for advanced oxidation of organic contaminants in aqueous solution.* Applied Catalysis B: Environmental, 2010. **100**(3-4): p. 529-534.

48. Song, Q., et al., *Catalytic carbon dioxide reforming of methane to synthesis gas over activated carbon catalyst.* Industrial & engineering chemistry research, 2008. **47**(13): p. 4349-4357.

49. Zhang, G., et al., *Catalytic performance of N-doped activated carbon supported cobalt catalyst for carbon dioxide reforming of methane to synthesis gas.* Journal of the Taiwan Institute of Chemical Engineers, 2018. **93**: p. 234-244.

50. Wong, F.F., et al., *Recovery and Reduction of Spent Alumina-Supported Cobalt–Molybdenum Oxide Catalyst via Plasma Sintering Technique.* Plasma Chemistry and Plasma Processing, 2008. **28**(3): p. 353-363.

Chapter 5

Conclusions and Recommendations

5.1 Conclusions

The activated carbon derived from hemp leaves is used as catalyst support for nickel and cobalt catalysts. The catalyst is synthesized in different optimum conditions and all catalyst samples were investigated one by one for SMR in a fixed bed reactor at 750 °C temperature. Initially, all samples, the catalyst, and support were operated for 8 h running time where methane conversion and production of hydrogen and CO were recorded sequentially. The material recorded as the best results is tested for catalyst stability. In our case, monometallic cobalt catalyst (5%Co@AC) gives better results in methane conversion and hydrogen production. Although the hydrogen production is noted with a bigger difference among all test materials. However, the methane conversion of the cobalt catalyst is considerably good than other materials. In most cases, the bimetallic catalyst gives the best results. However, in some cases, the monometallic catalyst also performs considerably well. The reason is a larger metal crystallite favours the carbon deposition that deteriorates the long-term catalyst performance and becomes the reason for catalyst deactivation hampering the catalyst stability. Whereas the catalysts with smaller metal crystallites do not deposit the carbon too much which disturbs the catalytic activity thus giving more stability and fewer chances of catalyst deactivation in the process. The high dispersion of metal over the catalyst support also describes the better activity of the catalyst. As it is clear from the XRD and SEM results of the Cobalt catalyst that high is observed in this case. The activated carbon derived Ni-Co@AC is synthesized and employed effectively for SRM to Syngas in a fixed bed reactor. The activated carbon derived catalyst is characterised successfully and found suitable for SRM. The addition of 5 wt% Co enhanced the methane conversion from 82.96% to 97.69%. The activated-derived catalyst is economical and greener approach for SRM

5.2 Recommendations

All synthesized materials are investigated for SMR for better syngas production on a fixed bed reactor. In the objective high methane conversion and better selectivity of hydrogen are expected in the study. Moreover, all samples are studied under various characterization techniques including XRD, BET, TGA, SEM-EDX, and FTIR. To the best of our knowledge, there is no previous work done on monometallic and bimetallic Ni-Co specifically impregnated on hemp leaves-derived AC for SMR reactions. However, there is considerable literature on monometallic and bimetallic Ni-Co for other reforming techniques besides SMR. Moreover, there is considerable literature found on hemp bast and fibre for AC production whereas hardly any literature found on AC from hemp leaves. The effect of different experimental parameters on the activity of hemp derived catalyst should be studied. Also, the kinetic study and reaction mechanism for hemp derived catalyst should be investigated.

Appendix-A

‘’Steam methane reforming over bimetal loaded hemp derived activated carbon-based catalyst for hydrogen production’’. Rashid Minhas [1], Asif Hussain Khoja [1], Salman Raza Naqvi[2], Rahat Javaid[3], Umair Yaqub Qazi[4*], Israf Ud Din[5]

MDPI_Energies(Under Review)(IF=3.25)

Manuscript ID	Journal	Section / Special Issue	Title	Status	Submission Date
energies-1779482	Energies	SI: Advances in CO₂-Free Energy Technologies	Steam methane reforming over bimetal loaded hemp derived activated carbon-based catalyst for hydrogen production	Under review	2022-06-03 15:45:11